Time-resolved photoelectron angular distributions as a probe of coupled polyatomic dynamics

Tamar Seideman
Steacie Institute for Molecular Sciences, National Research Council of Canada, Ottawa, Ontario K1A 0R6, Canada
(Received 21 February 2001; published 13 September 2001)

A nonperturbative theory for calculating time-resolved photoelectron angular distributions in linear molecules [J. Chem. Phys. **107**, 7859 (1997)] is extended to nonlinear systems and reformulated so as to expose and utilize the underlying electronic and rotational symmetries. A sequence of approximations is next introduced, systematically reducing the formally exact expression to cruder forms that are applicable to systems of increasing complexity. As an example of the potential applications of time-resolved photoelectron angular distributions in polyatomic dynamics we examine the information they convey about an ultrafast internal conversion.

DOI: 10.1103/PhysRevA.64.042504 PACS number(s): 33.60.Cv, 33.60.Fy, 34.30.+h, 34.90.+q

I. INTRODUCTION

Time-resolved methods are now an established complement to the more traditional tools of energy-resolved spectroscopy. The basic principle of the time-domain approach is simple and extremely general in application [1,2]. A first (pump) pulse prepares a nonstationary superposition of excited eigenstates. A second (probe) pulse interrogates the wave packet at a series of instances during its evolution. This concept has been applied, in the last three decades, to the study of a vast variety of problems in physics, chemistry, biology, and material science [1,2].

While the pump stage is straightforward and essentially universal, the design of a successful probe presents an interesting challenge and is often system and application dependent. Ideally, one desires that the probe scheme be specifically sensitive to those properties of the wave packet that carry the information sought. In addition, the process involved in probing the wave packet should be simple enough so as to merely serve as a template on the wave packet evolution, rather than contaminate the signal with its own dynamics.

With regard to the former criterion, the specific sensitivity of the probe, experience in the energy domain indicates that the better resolved the signal the more specific the information it contains. Thus, while in integrated pump-probe signals (such as total fluorescence spectroscopy, total mass spectrometry or total ionization spectroscopy) all-level spacings determining the wave packet evolution are entangled, observables that are resolved with respect to one or more properties of the detected species (e.g., dispersed fluorescence [1], translational-energy spectroscopy [3], or photoelectron spectroscopy [4–7]) are often capable of disentangling one motion from another. The latter criterion, the nonperturbing effect of the probe, is difficult to satisfy in practice and is evidently related to the former since the better resolved the signal the more sensitive it is also to the dynamics of the probe process. Below it will be useful to keep in mind that time-domain signals, even when partially resolved, are inevitably highly averaged as compared to frequency-domain signals. This averaging can be used for advantage.

Of particular interest to the present study are time-resolved ionization spectroscopies, which at present are becoming increasingly popular experimentally [4–6,8]. Similar to its energy-domain counterpart [9], time-domain ionization spectroscopy is sensitive to both the nuclear and the electronic dynamics and allows, at least in principle, resolution of either or both the photoelectron and the photoion signals with respect to energy, angle, and spin [10]. While the first of the above criteria is well satisfied, whether the second can be met is a difficult question; ionization is a complicated dynamical process, involving resonances, coupled-ion channels and complex interaction of the outgoing electron with the core. The difficulty of disentangling the ionization dynamics from the molecular information was noted in continuous-wave (cw) ionization studies and is clearly aggravated the better the ionization signal is resolved. The possibility of circumventing the complex nature of ionization processes to restore a simple physical picture for the wave packet evolution is addressed below (see also Ref. [11]).

The energy-resolved signal, i.e., the photoelectron energy distribution (PED) as a function of the pump-probe delay time, has been studied in some detail during the past few years [4–7]. Experimental and theoretical work illustrated the ability of time-resolved PEDs to map wave-packet vibrations [12,13], to follow in time the flow of energy between coupled vibrational modes [14] and the transfer of population between coupled electronic states [15–19], and to disentangle coupled electronic-vibrational dynamics [20,21].

Here we consider time-resolved photoelectron *angular* distributions as a complementary means of understanding coupling mechanisms in polyatomic excited states [22]. In the cw domain [23] the photoelectron angular distribution (PAD) has been long known to provide unique information about rotational level structures. Nanosecond studies [24,25] demonstrated the possibility of probing nuclear hyperfine coupling using PADs. Picosecond resolved PADs were shown to reflect rotation-vibration coupling [11,26–28].

Reference [29] proposed and illustrated theoretically the possibility of using femtosecond-resolved PADs to probe the dynamics of internal conversion processes. Very recently this opportunity was realized experimentally [30]. At present further experimental studies of ultrafast nonadiabatic dynamics are being set up in several other laboratories [31].

The problem of radiationless transitions (internal conversions and intersystem crossings) [32] plays a special role in molecular physics, this being one of the most-general phe-

nomena in excited-state dynamics [33], with fascinating consequences in the physics of vision and photosynthesis [34], and in molecular electronics [35]. Nonetheless, one may expect femtosecond-resolved PADs to provide a useful tool also in the study of other ultrafast phenomena in bound-state and dissociative dynamics [36–38]. From a theoretical perspective, femtosecond-pulses introduce several new features that do not play a role in the nanosecond regime. These are discussed in Ref. [39], where the nonperturbative formalism required for calculation of this observable is developed. More recently, numerical studies of femtosecond-resolved PADs from diatomic systems were also reported [11,40,41].

The ability of time-resolved PADs to map rotation-vibration energy transfer [26,27] owes to their sensitivity to the rotational composition of the wave packet [11,28]. The ability of the same observable to probe electronically nonadiabatic and spin-orbit coupling [30] owes to its sensitivity to the electronic symmetry of the probed state [29] (*vide infra*). By contrast to the former problem, the latter can, depending on the system, be studied also by measurement of time-resolved PEDs [15–21]. In practice we expect the two probes to be complementary in application. The energy-resolved probe relies on energetic difference between the coupled electronic states, which translates into a change of the photoelectron energy spectrum upon a nonradiative transition [15–21]. The angle-resolved probe relies on symmetry difference between the coupled electronic states, which translates, as shown below, into a change of the symmetry of the outgoing electronic waves in the course of a nonradiative transition [29].

Neither approach is completely general. As discussed in Refs. [15,20,21], the photoelectron kinetic-energy spectrum mirrors the electronic-energy content of the wave packet only if one of two conditions is met. Either the ion and neutral states should have similar equilibrium configurations, such that the vibrational energy of the neutral and ion states do not differ appreciably [15], or the coupled states should correlate upon ionization with different states of the ion [20]. In the case of angular distributions one requires that the coupled electronic states would differ in electronic symmetry. Group theoretical arguments, however, have the merit that their application requires little information about the system. Provided that the molecule is rigid on the time scale of the experiment [42], only the electronic symmetry of the states involved is needed in order to apply such arguments.

A second qualitative difference between the application of time-resolved PADs to the understanding of rotational perturbations and the application of the same observable to the understanding of nonradiative transitions needs to be noted. In the former case the study of simple systems is particularly helpful in exposing the physical origin of the mapping of the coupling forces into the observable [11,28]. The problem of nonradiative transitions inevitably involves the study of large polyatomic systems. The reason is three fold. First, it is typically in large molecules that level densities become large, frequency-domain spectra become difficult to interpret, and the time domain is expected to offer an advantage. Second, large systems, in particular, π-conjugated systems, offer large absorption and ionization cross sections in experimentally convenient regimes. Thus, time-resolved PED studies of nonradiative transitions have focused on systems such as aniline and aminopyridine [15], hexatriene [17], phenol [19], decatetraene [20], phenanthrene and naphthalene [21], and pyrazine [36]. Third, from the practical view point, one is interested in electronically coupled systems of relevance to photobiological processes [34] and to the design of future devices [35].

The above discussion exposes an important distinction between the ability of theory to predict accurately the effect of rotational perturbations on time-resolved PADs and its ability to predict with comparable accuracy the effect of electronic coupling. The former problem can be addressed within a single surface, single vibrational-mode calculation [11,28]. The latter involves the calculation of a vibronic Hamiltonian for a large polyatomic molecule and the propagation of a multidimensional ro-vibronic wave packet on coupled electronic surfaces, subject to laser fields that are typically nonperturbative. Furthermore, *ab initio* calculation of the electronic bound-free amplitudes (the matrix elements of the dipole operator between the bound and free-electronic states) for all relevant nuclear configurations, photoelectron energies, and photoelectron partial waves is difficult for three- and four-atom systems and impractical for large ones. For study of the former problem, as shown in Ref. [28], knowledge of these amplitudes is not essential. This result is intuitively expected since the process described depends on the nuclear, rather than on the electronic dynamics. In the case of nonradiative transitions the electronic wave functions carry the information sought and need be taken into account, even within a qualitative study.

The introduction of approximations is thus inevitable. The highly averaged (in the frequency sense) nature of time-resolved experiments in large systems [15,17–21] suggests that approximate theories, in particular theories that approximate the ionization dynamics (rather than the wave packet dynamics probed) could be also justified. The development of approximate models is useful, however, irrespective of whether their results match the accuracy of relevant experiments since they can provide physical insight into the properties and information content of the observable.

One of the purposes of the present work is to generalize the formalism of Ref. [39] to nonlinear polyatomic molecules and to reformulate the observable so as to expose and utilize the underlying electronic and rotational symmetries. A second goal is to systematically introduce a sequence of approximations that will allow the calculation of PADs for systems of chemical interest and provide transparent, closed-form expressions for the observables, that could serve as a basis for the interpretation of future measurements or accurate calculations. A third goal is to address specifically the problem of probing nonradiative transitions with PADs. With that we hope to guide future experiments as to the choice of molecular systems and field parameters.

The next section outlines the theory. We first (Sec. II A) extend the formalism [39] to nonlinear systems and motivate the use of time-resolved PADs as a probe of a time-evolving electronic symmetry. In Sec. II B we introduce a series of approximations, sequentially reducing the formally exact ex-

pression to simpler forms that could be applied to systems of increasing complexity. Section II B 6 briefly summarizes the approximations introduced in Secs. II B 1–II B 5, noting their range of validity. Readers uninterested in the formalism may want to skip Sec. II A and proceed directly to Sec. II B, where we focus on physical interpretation. Section III provides a numerical example and the final section concludes with an outlook to future research. All mathematical details are omitted from the text and collected in Appendices. Appendix A is devoted to group-theoretical arguments while Appendixes B–D outline the solution of integrals and the derivation of sum rules used in Sec. II.

II. THEORY

A. General formalism

We consider a molecular eigenstate subject to two sequential light pulses,

$$\vec{\varepsilon}_i(t)=\hat{\varepsilon}_i f_i(t)e^{-i\omega_i t}+\text{c.c.},\quad i=\text{pu,pr}, \tag{1}$$

where $\hat{\varepsilon}_i$ is a unit vector along the polarization direction, $f_i(t)$ is a smooth envelope, and ω_i is the central frequency.

The first (pump) pulse, $\vec{\varepsilon}_{\text{pu}}$, projects the initial eigenstate onto a superposition of rovibrational eigenstates of an electronically excited state. The second (probe) pulse, $\vec{\varepsilon}_{\text{pr}}$, couples the electronically excited state with the ionization continuum. Following Ref. [39] we expand the time-dependent wave packet in eigenstates of the field-free Hamiltonian, $H_0=H(t)+\Sigma_i\vec{\mu}\cdot\vec{\varepsilon}_i(t)$, as

$$\begin{aligned}|\Psi(t)\rangle=&\sum_{\xi=0,1}\sum_{n_\xi M_\xi} C_\xi^{n_\xi M_\xi}(t)|\xi\, n_\xi M_\xi\rangle\exp(-iE_\xi^{n_\xi}t)\\&+\sum_{n_c M_c}\int d\epsilon\int d\hat{k}\, C^{n_c M_c}(\epsilon\,\hat{k}\,t)|\epsilon\,\hat{k}\,n_c\,M_c\rangle\\&\times\exp[-i(E^{n_c}+\epsilon)t],\end{aligned} \tag{2}$$

where $\xi=0,1$ is an electronic index ($\xi=0$ is the initial electronic state and $\xi=1$ is that reached by the pump), n_ξ denotes collectively the energy-level indices, including the rovibrational quantum numbers and the electron spin, M_ξ is the magnetic quantum number, the projection of the total angular momentum J_ξ onto the space-fixed z axis, and $E_\xi^{n_\xi}$ is the eigenenergy. We denote by ϵ the photoelectron energy and by $\hat{k}=(\theta_k,\phi_k)$ the photoelectron ejection direction in the space-fixed frame. The subscript c denotes the core indices, we reserve the label $\xi=2$ to attributes of the ion+electron system.

Substituting Eq. (2) in the time-dependent Schrödinger equation and using the orthogonality of the field-free eigenstates, one obtains a set of coupled differential equations for the expansion coefficients,

$$\begin{aligned}i\dot{C}_0^{n_0M_0}(t)=&\sum_{n_1M_1}C_1^{n_1M_1}(t)\langle 0n_0M_0|\vec{\mu}\cdot\vec{\varepsilon}_{\text{pu}}(t)|1n_1M_1\rangle\\&\times\exp[i(E_0^{n_0}-E_1^{n_1})t],\end{aligned} \tag{3}$$

$$\begin{aligned}i\dot{C}_1^{n_1M_1}(t)=&\sum_{n_0M_0}C_0^{n_0M_0}(t)\\&\times\langle 1n_1M_1|\vec{\mu}\cdot\vec{\varepsilon}_{\text{pu}}(t)|0n_0M_0\rangle\exp[i(E_1^{n_1}-E_0^{n_0})t]\\&+\sum_{n_cM_c}\int d\epsilon\int d\hat{k}C^{n_cM_c}(\epsilon\hat{k}t)\\&\times\langle 1n_1M_1|\vec{\mu}\cdot\vec{\varepsilon}_{\text{pr}}(t)|\epsilon\hat{k}n_cM_c\rangle\\&\times\exp[i(E_1^{n_1}-E^{n_c}-\epsilon)t],\end{aligned} \tag{4}$$

and

$$\begin{aligned}i\dot{C}^{n_cM_c}(\epsilon\hat{k}t)=&\sum_{n_1M_1}C_1^{n_1M_1}(t)\langle\epsilon\hat{k}n_cM_c|\vec{\mu}\cdot\vec{\varepsilon}_{\text{pr}}(t)|1n_1M_1\rangle\\&\times\exp[i(E^{n_c}+\epsilon-E_1^{n_1})t],\end{aligned} \tag{5}$$

supplemented by a set of initial conditions, $C_\xi^{n_\xi M_\xi}(t=0)=\delta_{\xi,0}\delta_{n_\xi,n_i}\delta_{M_\xi,M_i}$ [43]. In general the two pulses do not overlap in time and hence Eqs. (3)–(5) separate into two sets of equations, one describing the dynamics during the pump stage [$\vec{\varepsilon}_{\text{pr}}(t)=0$] and the second corresponding to the dynamics during the probe stage [$\vec{\varepsilon}_{\text{pu}}(t)=0$].

The state-, time-, and angle-resolved cross section is given as the squared modulus of the corresponding continuum amplitude,

$$\sigma(\overline{\epsilon}\hat{k}n_cM_c|\Delta t|n_iM_i)=\lim_{t\to\infty}\int d\epsilon|C^{n_cM_c}(\epsilon\hat{k}t)|^2, \tag{6}$$

where Δt is the delay time, the difference between the centers of the pump and probe pulses, and integration is over the range of photoelectron-energies spanned by the probe band width. We denote by $\overline{\epsilon}$ an averaged photoelectron energy, defined to within the energy resolution and upper limited through energy conservation, $\overline{\epsilon}\leqslant E_0^{n_i}+\omega_{\text{pu}}+\omega_{\text{pr}}-E^{n_c}$.

In time-resolved experiments, in particular for large molecules, the measurable is typically not the fully resolved cross section of Eq. (6) but a rather less-detailed cross section, summed over the magnetic (M_c) and rotational (J_c) states of the core [and usually also over several vibrational (v_c) levels] and averaged over the initial magnetic (M_i) levels and over a Boltzmann distribution of initial ro-vibrational states. Below we determine analytically the forms of the partially averaged cross sections,

$$\overline{\sigma}(\overline{\epsilon}\hat{k}n_c|\Delta t|n_i)=\frac{1}{2J_i+1}\sum_{M_iM_c}\sigma(\overline{\epsilon}\hat{k}n_cM_c|\Delta t|n_iM_i), \tag{7}$$

and

$$\overline{\overline{\sigma}}(\overline{\epsilon\hat{k}}n_c|\Delta t|n_i)=\sum_{J_c}\overline{\sigma}(\overline{\epsilon\hat{k}}n_c|\Delta t|n_i), \tag{8}$$

from which all further averaged observables are obtained numerically.

In order to provide explicit expressions for the coupling matrix elements, $\langle 1n_1M_1|\vec{\mu}\cdot\vec{\varepsilon}_{\rm pu}(t)|0n_0M_0\rangle$ and $\langle \epsilon\hat{k}n_cM_c|\vec{\mu}\cdot\vec{\varepsilon}_{\rm pr}(t)|1n_1M_1\rangle$ in Eqs. (3)–(5), we proceed to identify the forms of the field-free eigenstates and the field-matter interaction. The bound and continuum states are written in a Hund's case (b) basis as

$$|\xi n_\xi M_\xi\rangle=|\xi\rangle|n_\xi\rangle\tilde{J}_\xi(-1)^{N_\xi-S_\xi+M_\xi}\times\sum_{M_{N_\xi}M_{S_\xi}}\begin{pmatrix}N_\xi & S_\xi & J_\xi\\ M_{N_\xi} & M_{S_\xi} & -M_\xi\end{pmatrix}\times|S_\xi M_{S_\xi}\rangle|N_\xi\tau_\xi M_{N_\xi}p_\xi\rangle,\quad \xi=0,1 \tag{9}$$

and

$$|\epsilon\hat{k}n_cM_c\rangle=|\epsilon\hat{k}\rangle|n_c\rangle\tilde{J}_c(-1)^{N_c-S_c+M_c}\times\sum_{M_{N_c}M_{S_c}}\begin{pmatrix}N_c & S_c & J_c\\ M_{N_c} & M_{S_c} & -M_c\end{pmatrix}\times|S_cM_{S_c}\rangle|N_c\tau_cM_{N_c}p_c\rangle \tag{10}$$

where $\tilde{J}=\sqrt{2J+1}$, N are total angular momenta excluding spin, M_N are the corresponding space-fixed z projections and M_S are the projections of the spin angular momenta onto the space-fixed z axis. We assume, in Eqs. (9) and (10), that spin-orbit and Coriolis interactions do not come into play on the time scale of the phenomena to be studied. The $\langle\mathbf{Q};\mathbf{R}|\xi\rangle$ and $\langle\mathbf{Q};\mathbf{R}|\epsilon\hat{k}\rangle$ are electronic functions, parametrically dependent on the nuclear configuration, the $\langle\mathbf{R}|n_\xi\rangle$ are vibrational eigenfunctions and the $\langle\hat{R}|N\tau M_Np\rangle$ are eigenfunctions of the rotational Hamiltonian. We denote by $\mathbf{Q}$ the electronic coordinates, defined with respect to the body-fixed frame, $\mathbf{R}$ are the nuclear coordinates, and $\hat{R}=(\phi,\theta,\nu)$ are the Euler angles of rotation of the body-fixed frame with respect to the space-fixed frame. Throughout this paper we denote coordinates defined with respect to the body-fixed and space-fixed frames by capital and small letters, respectively.

The rotational eigenstates are given as

$$|N\tau M_Np\rangle=\sum_K a_{N\tau K}|NKM_Np\rangle, \tag{11}$$

where $\tau=-N,-N+1,\ldots,N$, $|NKM_Np\rangle$ are symmetry-adapted symmetric-top functions, satisfying the symmetries of the D_2 group [45,46],

$$|NKM_Np\rangle=\frac{1}{\sqrt{2}}(|NKM_N\rangle+(-1)^p|N-KM_N\rangle),\quad p=0,1 \tag{12}$$

and $|NKM_N\rangle$ are standard symmetric-top states,

$$\langle\hat{R}|NKM_N\rangle=\sqrt{\frac{2N+1}{8\pi^2}}D^{N*}_{M_NK}(\hat{R}). \tag{13}$$

(Although the notation of Edmonds [47] was used in our earlier work on this subject [11,39,40,28], we adopt here the notation of Zare [46] since Ref. [46] is becoming increasingly popular.) The continuum electronic states in Eq. (10) are expanded as

$$\langle\mathbf{Q};\mathbf{R}|\epsilon\hat{k}\rangle=\sqrt{\frac{2}{\pi}}\sum_{m_s}\left|\frac{1}{2}\ m_s\right\rangle\times\sum_{\gamma\mu hl}i^l\langle\mathbf{Q};\mathbf{R}|\epsilon\gamma\mu hl\rangle X^{\gamma\mu*}_{hl}(\hat{K}), \tag{14}$$

where m_s is the electron spin, $\hat{K}$ denotes the direction of ejection of the electron in the body-fixed frame, and $X^{\gamma\mu}_{hl}$ are generalized harmonics [48–50], satisfying the symmetries of the molecular point group [51],

$$X^{\gamma\mu}_{hl}(\hat{K})=\sum_{k_l}b^{\gamma\mu}_{hlk_l}Y_{lk_l}(\hat{K}). \tag{15}$$

In Eq. (15) γ denotes the irreducible representation (IR), μ distinguishes between components of the IR if its dimension is larger than one, and h distinguishes between different bases of the IR corresponding to the same electron angular momentum l. Generalized harmonics were found numerically advantageous in solid-state calculations [48] as well as in studies of electron scattering [49] and molecular ionization [50,52]. In the present study they are used primarily for conceptual purposes, as discussed below. The properties of the generalized harmonics for several point groups of current experimental interest, and their implications to the form of the photoelectron distribution in the molecular frame are discussed in Appendix A. The form of the bound electronic state, $\langle\mathbf{Q};\mathbf{R}|\xi\rangle$ in Eq. (9), and the expansion coefficients, $\langle\mathbf{Q};\mathbf{R}|\epsilon\gamma\mu hl\rangle$ in Eq. (14), are system dependent and discussed in Sec. II B 5. Here we note only that both functions transform according to the various IRs of the molecular point group [51].

The field-matter interaction in Eqs. (3)–(5) is usually expanded in spherical unit vectors [53],

$$\vec{\mu}\cdot\hat{\varepsilon}=\sum_{qs}\varepsilon_q\mu_sD^{1*}_{qs}(\hat{R}),\quad \mu_s=\sqrt{\frac{4\pi}{3}}\sum_\nu q_\nu Y_{1s}(\hat{Q}_\nu), \tag{16}$$

where Eq. (9) of Ref. [53] is written in the notation of Ref. [46], ν labels the electrons, and Y_{lm} are spherical harmonics. For our present purpose it is advantageous to express Eq. (16) in terms of Cartesian vectors ($\rho=X,Y,Z$) that transform

as the symmetry-adapted rotation matrices of Eq. (12),

$$\vec{\mu}\cdot\hat{\varepsilon}=\sqrt{\frac{8\pi^2}{3}}\sum_q \varepsilon_q \sum_{\rho=X,Y,Z}\sum_\nu \mu_\rho \rho_\nu \langle \hat{R}|1k_\rho q p_\rho\rangle, \tag{17}$$

where the μ_ρ are phase factors, $\mu_X=-1$, $\mu_Y=-i$, $\mu_Z=1$, and the k_ρ and p_ρ describe the symmetry of the Cartesian coordinates with respect to the operations of the D_2 group; $k_X=k_Y=1$, $k_Z=0$, $p_X=1$, and $p_Y=p_Z=0$.

Using Eqs. (9), (10), (14), and (17) we have

$$\begin{aligned}&\langle 1n_1M_1|\vec{\mu}\cdot\hat{\varepsilon}_{\rm pu}|0n_0M_0\rangle\\ &=\sum_{q\rho_{10}}\varepsilon_q \sum_{M_{N_1}M_{N_0}M_{S_1}M_{S_0}}(-1)^{N_1-S_1+M_1+N_0-S_0+M_0}\tilde{J}_1\tilde{J}_0\begin{pmatrix}N_1 & S_1 & J_1\\ M_{N_1} & M_{S_1} & -M_1\end{pmatrix}\\ &\times\begin{pmatrix}N_0 & S_0 & J_0\\ M_{N_0} & M_{S_0} & -M_0\end{pmatrix}W(N_1\tau_1M_{N_1}p_1|k_{10}qp_{10}|N_0\tau_0M_{N_0}p_0)T(n_1|\rho_{10}|n_0)\end{aligned} \tag{18}$$

and

$$\begin{aligned}&\langle \epsilon\hat{k}n_cM_c|\vec{\mu}\cdot\hat{\varepsilon}_{\rm pr}|1n_1M_1\rangle\\ &=\sum_{q\rho_{21}}\varepsilon_q \sum_{M_{N_c}M_{N_1}M_{S_c}M_{S_1}}(-1)^{N_c-S_c+M_c+N_1-S_1+M_1}\tilde{J}_c\tilde{J}_1\begin{pmatrix}N_c & S_c & J_c\\ M_{N_c} & M_{S_c} & -M_c\end{pmatrix}\\ &\times\begin{pmatrix}N_1 & S_1 & J_1\\ M_{N_1} & M_{S_1} & -M_1\end{pmatrix}\sum_{\gamma\mu hlk_lm_l}Y_{lm_l}(\hat{k})b^{\gamma\mu}_{hlk_l}W(N_c\tau_cM_{N_c}p_c|lk_lm_l|k_{21}qp_{21}|N_1\tau_1M_{N_1}p_1)\\ &\times T(n_c|\epsilon\gamma\mu hl|\rho_{21}|n_1),\end{aligned} \tag{19}$$

where

$$\begin{aligned}&W(N_1\tau_1M_{N_1}p_1|k_{10}qp_{10}|N_0\tau_0M_{N_0}p_0)\\ &=\sqrt{\frac{8\pi^2}{3}}\int d\hat{R}\langle\hat{R}|N_1\tau_1M_{N_1}p_1\rangle^*\\ &\times\langle\hat{R}|1k_{10}qp_{10}\rangle\langle\hat{R}|N_0\tau_0M_{N_0}p_0\rangle,\end{aligned} \tag{20}$$

$$T(n_1|\rho_{10}|n_0)=\langle n_1|I(\rho_{10})|n_0\rangle, \tag{21}$$

$$I(\rho_{10};\mathbf{R})=\sum_\nu \langle 1|\rho_{\nu,10}|0\rangle\mu_{\rho_{10}}, \tag{22}$$

$$\begin{aligned}&W(N_c\tau_cM_{N_c}p_c|lk_lm_l|k_{21}qp_{21}|N_1\tau_1M_{N_1}p_1)\\ &=\sqrt{\frac{8\pi^2}{3}}\int d\hat{R}\langle\hat{R}|N_c\tau_cM_{N_c}p_c\rangle^*D^l_{m_lk_l}(\hat{R})\\ &\times\langle\hat{R}|1k_{21}qp_{21}\rangle\langle\hat{R}|N_1\tau_1M_{N_1}p_1\rangle,\end{aligned} \tag{23}$$

$$T(n_c|\epsilon\gamma\mu hl|\rho_{21}|n_1)=\langle n_c|I(\epsilon\gamma\mu hl|\rho_{12})|n_1\rangle, \tag{24}$$

and

$$I(\epsilon\gamma\mu hl|\rho_{12};\mathbf{R})=\sqrt{\frac{2}{\pi}}\,i^{-l}\sum_\nu \langle\epsilon\gamma\mu hl|\rho_{\nu,21}|1\rangle\mu_{\rho_{21}}. \tag{25}$$

In Eqs. (18)–(20) and (23), k_{10} and p_{10} are shorthand for $k_{\rho_{10}}$ and $p_{\rho_{10}}$ and similarly k_{21} and p_{21}. The W of Eqs. (20) and (23) contain the details of the rotational Hamiltonian in the initial, excited, and ion state and the selection rules, determined by the field polarization and the nature of the transition. The T in Eqs. (21) and (24) contain the details of the vibrational Hamiltonian. In the case of electronically coupled systems, this includes the potential- and kinetic-energy functions in all electronic states involved and their coupling, usually written in a diabatic representation. The I, Eqs. (22) and (25), account for the electron-scattering dynamics and for the symmetry of the bound and free-electronic wave functions. In particular, $I(\epsilon\gamma\mu hl|\rho_{21};\mathbf{R})$ vanishes unless the integrand in Eq. (25) is invariant under the operation of all elements of the point group [51] of the molecular Hamiltonian [44]. The integration over the Euler angles in Eqs. (20) and (23) is readily carried out analytically, as shown in Appendix B. The integration over the dynamical variables in Eqs. (21), (22), (24), and (25) need be performed numerically in general.

Implicit in our use of point-group symmetry and a semirigid rotational Hamiltonian [54] is the assumption that tunneling between equivalent equilibrium conformations does not take place on the time scale of the experiment. This

assumption normally holds for the fast phenomena considered here. The formalism can be extended to study problems where large-amplitude motion plays a role, and cases where the equilibria of electronic states involved belong to different point groups, by application of molecular symmetry groups and a nonrigid rotation-vibration Hamiltonian (see Ref. [55] for examples).

Equations (18)–(25) are general, applying to all-32 molecular point groups. To proceed one needs to specify the point group of the molecule, which determines the form of the generalized harmonics in Eq. (15) and the symmetry properties of the electronic functions and dipole operators in Eqs. (22) and (25). Inspection of the point-groups character-tables [44] indicates that for all point groups that do not have rotation axes of order higher than 2 (C_1, C_2, C_i, C_{2h}, D_2, C_{2v}, and D_{2h}) Eq. (15) reduces to

$$X^{\gamma}_{lk_l}=\frac{1}{\sqrt{2}}(Y_{lk_l}+(-1)^{p_\gamma}Y_{l-k_l}),\quad p_\gamma=0,1, \tag{26}$$

which, as expected, is of the form of Eq. (12). Systems of current experimental interest include long-chain transpolyenes [20,21] and azulene; which belongs to C_{2h}, phenanthrene [21], cis-hexatriene [17], and phenol [19]; which belong to C_{2v} and naphthalene [21] and pyrazine [36]; which belong to D_{2h}. Femtosecond-resolved PEDs of the former systems have been already measured and one expects current technology to allow also the observation of angular distributions. For pyrazine measurements of PADs were recently reported [36]. For these systems the electronic symmetry is described by Eq. (26) and, using the theory of successive rotations [46], one finds

$$X^{\gamma}_{lk_l}(\hat{K})=\sqrt{\frac{8\pi^2}{2l+1}}\sum_{m_l}\langle\hat{R}|lk_lm_lp_\gamma\rangle^*Y_{lm_l}(\hat{k}). \tag{27}$$

As shown in Appendix B, the geometric functions W in Eq. (19) assume with Eq. (27) a particularly symmetric and physically transparent form that offers a numerical advantage also.

B. Successive approximations and physical interpretation

Together with Eqs. (18)–(25), Eqs. (6)–(8) provide formally exact expressions for the time-resolved PAD of a general polyatomic molecule, nonperturbative in both the pump and the probe fields as well as in the nonradiative interaction. We proceed by introducing a series of simplifying approximations, to derive a form that provides better insight and is easier to deal with numerically.

1. Golden-rule approximation

In principle, nonperturbative treatment of both the pump and the probe fields is necessary since short-pulse experiments in the gas phase are generally associated with high-laser intensities. This is particularly true when the probe stage is multiple resolved. As discussed in Sec. IV, the intensity property characteristic of short pulses needs to be taken into considerations not only since it may complicate the interpretation of data but also since it can be used for advantage.

Depending on the system and on the observable; however, it is often possible and desirable to minimize strong-field effects. Reference [40] examines in detail the role played by the pump and probe intensities in determining the time-resolved PAD. It is found that the probe intensity does not alter the form of the PAD (although its magnitude is strongly affected) within the range typical of pump-probe experiments in chemical systems. The origin of this counter-intuitive result is explored in Ref. [40] and is expected to hold more generally. The intensity of the pump field is usually important to account for, in particular if angular distributions are the observable, due to the phenomenon of rotational excitation in strong fields [56], which is most clearly observed in the PAD. The degree of rotational excitation, however, is upper bounded by the pump duration ($\tau_{\rm pu}$) [56], $J^{\max}\sim\tau_{\rm pu}\Omega_R^{J^{\max}}$, Ω_R being the Rabi coupling. In cases where the intensity or the pump duration can be reduced such that $\tau_{\rm pu}<\Omega_R^{-1}$ rotational excitation is negligible.

It is useful to examine the weak-field limit regardless of its relevance to experiments so as to simplify the derivation of analytical expressions for the angle and time dependencies of the observable. Within first-order perturbation theory and the rotating-wave approximation Eq. (6) reduces to [39]

$$\begin{aligned}\sigma^{\rm PT}(\vec{\epsilon}\hat{k}n_cM_c|\Delta t|n_iM_i)&=4\pi^2\int d\epsilon\Big|\sum_{n_1,M_1}\langle\epsilon\hat{k}n_cM_c|\vec{\mu}\cdot\hat{\varepsilon}_{\rm pr}|1n_1M_1\rangle\\&\times\langle1n_1M_1|\vec{\mu}\cdot\hat{\varepsilon}_{\rm pu}|0n_iM_i\rangle\tilde{\varepsilon}_{\rm pr}(E^{n_c}+\epsilon-E_1^{n_1})\\&\times\tilde{\varepsilon}_{\rm pu}(E_1^{n_1}-E_0^{n_i})\Big|^2,\end{aligned} \tag{28}$$

where $\tilde{\varepsilon}_i(\omega)$, $i={\rm pu,pr}$, are the Fourier transforms of the pump- and probe-pulse envelopes, respectively, and the superscript PT stands for perturbation theory. In the weak-field limit $n_0=n_i$, $M_0=M_i$, and the excited and ion rotational and magnetic levels are determined by the single-photon selection rules and the polarization of the pump and probe electric fields.

The dependence of the bound-bound and bound-free matrix elements on the initial (M_i), intermediate (M_1), core (M_c), and photoelectron (m_l) magnetic states is of geometrical (rather than dynamical) origin and hence involves only analytical functions. It follows that summation of Eq. (28) over the magnetic components can be carried out analytically. The details are given in Appendix C. Confining attention to the case of linearly polarized, parallel pump and probe field vectors ($q=0$, $\hat{\varepsilon}_{\rm pu}=\hat{\varepsilon}_{\rm pr}$) and, for simplicity of notation, neglecting the spin variables one obtains for the partially summed cross section of Eq. (7),

$$\overline{\sigma}^{\mathrm{PT}}(\overline{\epsilon\hat{k}}n_c|\Delta t|n_i)=\frac{1}{2J_i+1}\sum_{M_cM_i}\sigma^{\mathrm{PT}}(\overline{\epsilon\hat{k}}n_cM_c|\Delta t|n_iM_i)$$

$$=4\pi^2\sum_{n_1n_1'}\sum_{\rho_{10}\rho_{10}'}T(n_1|\rho_{10}|n_i)T^*(n_1'|\rho_{10}'|n_i)w(J_1\tau_1p_1|k_{10}p_{10}|J_i\tau_ip_i)w(J_1'\tau_1'p_1'|k_{10}'p_{10}'|J_i\tau_ip_i)$$

$$\times\sum_{\rho_{21}\rho_{21}'}\sum_{\gamma lk_l\gamma' l'k_l'}\int d\epsilon T(n_c|\epsilon\gamma lk_l|\rho_{21}|n_1)T^*(n_c|\epsilon\gamma' l'k_l'|\rho_{21}'|n_1')$$

$$\times\sum_{J_2J_2'}w(J_2|J_c\tau_cp_c|lk_lp_\gamma|k_{21}p_{21}|J_1\tau_1p_1)w(J_2'|J_c\tau_cp_c|l'k_l'p_{\gamma'}|k_{21}'p_{21}'|J_1'\tau_1'p_1')\tilde{\varepsilon}_{\mathrm{pu}}(E_1^{n_1}-E_0^{n_i})$$

$$\times\tilde{\varepsilon}_{\mathrm{pu}}^*(E_1^{n_1'}-E_0^{n_i})\tilde{\varepsilon}_{\mathrm{pr}}(E^{n_c}+\epsilon-E_1^{n_1})\tilde{\varepsilon}_{\mathrm{pr}}^*(E^{n_c}+\epsilon-E_1^{n_1'})\sum_{j=0,2,4}F_j(J_iJ_1J_1'll'J_2J_2'J_c)P_j(\cos\theta_k), \quad (29)$$

where $w(J_1\tau_1p_1|\rho_{10}|J_i\tau_ip_i)$ and $w(J_2|J_c\tau_cp_c|lk_lp_\gamma|\rho_{21}|J_1\tau_1p_1)$ are given by Eqs. (B2) and (B4), F_j is given by Eq. (C8), and P_j are Legendre polynomials. Thus, the M_c summed, M_i-averaged PAD takes the form

$$\overline{\sigma}^{\mathrm{PT}}=\frac{\sigma_{\mathrm{tot}}^{\mathrm{PT}}(\Delta t)}{4\pi}[1+\beta_2(\Delta t)P_2(\cos\theta_k)+\beta_4(\Delta t)P_4(\cos\theta_k)], \quad (30)$$

where we indicate explicitly the dependence of the integral cross section σ_{tot} and the asymmetry parameters β_j on the delay time.

Equation (30) may have been anticipated since, from the view point of angular momentum algebra, a pump-probe experiment is equivalent to a two-photon process in the weak-field limit. It is worth pointing out that the cylindrical symmetry of Eq. (30) results from our choice of parallel polarization axes of the pump and probe fields. With noncollinear polarization axes, interference between magnetic components of the electronic wave function ($m_l'\neq m_l$) gives rise to dependence of the PAD on the azimuthal scattering angle ϕ_k, providing complementary information about the electronic symmetry of the wave packet. The form of the M_c-summed, M_i-averaged PAD in a nonperturbative field is derived in Ref. [22].

2. Slowly varying continuum approximation

While energy-dependence of the bound-free electronic amplitudes in Eq. (25) is in general important to account for, within the narrow range spanned by the probe pulse it is negligible except in the vicinity of sharp resonances. In practice the application of time-resolved PADs as a probe requires that one tunes away from resonances (otherwise the signal is determined by the ionization dynamics, rather than by the wave packet motion). Neglect of the ϵ dependence of the $T(n_c|\epsilon\gamma lk_l|\rho_{21}|n_1)$ in comparison with the rapidly oscillating term $\tilde{\varepsilon}_{\mathrm{pr}}(E^{n_c}+\epsilon-E_1^{n_1})$ is thus a valid approximation. For a Gaussian pulse one finds

$$\overline{\sigma}^{\mathrm{SVCA}}(\overline{\epsilon\hat{k}}n_c|\Delta t|n_i)=\sqrt{\frac{\pi^5}{2}}\varepsilon_{\mathrm{pr}}^2\tau_{\mathrm{pr}}\sum_{n_1n_1'}\sum_{\rho_{10}\rho_{10}'}T(n_1|\rho_{10}|n_i)T^*(n_1'|\rho_{10}'|n_i)$$

$$\times w(J_1\tau_1p_1|k_{10}p_{10}|J_i\tau_ip_i)w(J_1'\tau_1'p_1'|k_{10}'p_{10}'|J_i\tau_ip_i)$$

$$\times\sum_{\rho_{21}\rho_{21}'}\sum_{\gamma lk_l\gamma' l'k_l'}T(n_c|\overline{\epsilon}\gamma lk_l|\rho_{21}|n_1)T^*(n_c|\overline{\epsilon}\gamma' l'k_l'|\rho_{21}'|n_1')$$

$$\times\sum_{J_2J_2'}w(J_2|J_c\tau_cp_c|lk_lp_\gamma|k_{21}p_{21}|J_1\tau_1p_1)w(J_2'|J_c\tau_cp_c|l'k_l'p_{\gamma'}|k_{21}'p_{21}'|J_1'\tau_1'p_1')$$

$$\times f_{\mathrm{pu}}(E_1^{n_1}-E_0^{n_i})f_{\mathrm{pu}}(E_1^{n_1'}-E_0^{n_i})\exp\left[-\frac{\tau_{\mathrm{pr}}^2}{8}(E_1^{n_1}-E_1^{n_1'})^2\right]\exp[-i(E_1^{n_1}-E_1^{n_1'})\Delta t]$$

$$\times\sum_{j=0,2,4}F_j(J_iJ_1J_1'll'J_2J_2'J_c)P_j(\cos\theta_k), \quad (31)$$

where $\tau_{\rm pr}$ and $\varepsilon_{\rm pr}$ are the duration and amplitude of the probe pulse, respectively, and $f_{\rm pu}(\omega)$ are real arithmetic amplitudes defined as [39],

$$f_{\rm pu}(\omega)=\frac{1}{\sqrt{2\pi}}\int_{-\infty}^{\infty}dt\, f_{\rm pu}(t)e^{i(\omega-\omega_{\rm pu})(t-t_{\rm pu})}.$$

Equation (31) shows explicitly the generic sinusoidal Δt dependence, common to all pump-probe signals, and is manifestly real. This can be seen by reexpressing $\overline{\sigma}^{\rm SVCA}(\overline{\epsilon}\hat{k}n_c|\Delta t|n_i)$ as

$$\begin{aligned}\overline{\sigma}^{\rm SVCA}(\overline{\epsilon}\hat{k}n_c|\Delta t|n_i)&=\sqrt{\frac{\pi^5}{2}}\varepsilon_{\rm pr}^2\tau_{\rm pr}\sum_{\eta,\eta'}B_\eta B_{\eta'}^*\exp\left[-\frac{\tau_{\rm pr}^2}{8}(E_1^{n_1}-E_1^{n_1'})^2\right]\\&\times\exp[-i(E_1^{n_1}-E_1^{n_1'})\Delta t]\sum_{j=0,2,4}F_j(J_iJ_1J_1'll'J_2J_2'J_c)P_j(\cos\theta_k)\\&=\sqrt{\frac{\pi^5}{2}}\varepsilon_{\rm pr}^2\tau_{\rm pr}\sum_{\eta}\sum_{\eta'\le\eta}\frac{1}{1+\delta_{\eta,\eta'}}|B_\eta B_{\eta'}^*|\exp\left[-\frac{\tau_{\rm pr}^2}{8}(E_1^{n_1}-E_1^{n_1'})^2\right]\\&\times\cos[(E_1^{n_1}-E_1^{n_1'})\Delta t+\Phi_{\eta,\eta'}]\sum_{j=0,2,4}F_j(J_iJ_1J_1'll'J_2J_2'J_c)P_j(\cos\theta_k),\end{aligned}\tag{32}$$

where

$$\begin{aligned}B_\eta\equiv&T(n_1|\rho_{10}|n_i)w(J_1\tau_1p_1|k_{10}p_{10}|J_i\tau_ip_i)\\&\times T(n_c|\overline{\epsilon}\gamma lk_l|\rho_{21}|n_1)w(J_2|J_c\tau_cp_c|lk_lp_\gamma|k_{21}p_{21}|\\&\times J_1\tau_1p_1)f_{\rm pu}(E_1^{n_1}-E_0^{n_i}),\end{aligned}\tag{33}$$

and $\Phi_{\eta,\eta'}=\arg\{B_\eta B_{\eta'}^*\}$.

3. A short-time approximation

Although nonradiative transitions take place on a wide range of time scales, the case of ultrafast (few hundreds of femtosecond) processes, more typical of internal conversion, is particularly suitable for time-domain studies and relevant for applications [34,35]. From the chemical view point, study of electronically nonadiabatic processes taking place on the time scale of molecular vibrations is of special interest in that it opens the possibility of observing the transfer of electronic energy into vibrational excitation. We proceed to show that the time-resolved PAD simplifies substan-tially if attention is focused on fast processes, where ''fast'' is quantified below.

In Eq. (31), the rotational and vibrational motions are entangled (although Coriolis interactions are excluded) due to centrifugal forces (dependence of the rotational Hamiltonian on vibrations [54]). Such perturbations are associated with small-energy splittings and, in the time domain, give rise to observable effects on long time scales [11,28]. With centrifugal coupling neglected, $\langle\mathbf{R}|n_\xi\rangle$ in Eqs. (9) and (10) are independent of J_ξ. For heavy systems the dependence of $E_\xi^{n_\xi}$ on J_ξ is small, at least within the narrow range of dipole allowed J_1 and J_c. We proceed by neglecting the dependence of both body-fixed eigenstates and the corresponding eigenvalues on the intermediate and ion-state angular momenta. As shown in Appendix D, this approximation separates the cross section into rotational and vibrational terms where the former consist of analytical functions only. It follows that summation of the cross section over the ion rotational states [Eq. (8)] as well as the coherent sums over J_1 and J_2 in Eq. (31) can be performed analytically, significantly simplifying the form of the PAD. Confining attention to the case of a symmetric top and using Eqs. (D1)–(D5) we have

$$\begin{aligned}\overline{\overline{\sigma}}^{\rm ST}(\overline{\epsilon}\hat{k}v_c|\Delta t|n_i)&\approx\sum_{J_c,K_c}\overline{\sigma}^{\rm svca}(\overline{\epsilon}\hat{k}n_c|\Delta t|n_i)\\&=\sum_{v_1v_1'}G(v_1v_1'n_i|\Delta t)\sum_{\rho_{10}\rho_{10}'}T(v_1|\rho_{10}|n_i)T^*(v_1'|\rho_{10}'|n_i)\\&\times\sum_{\rho_{21}\rho_{21}'}\sum_{\gamma lk_l\gamma' l'k_l'}T(v_c|\overline{\epsilon}\gamma lk_l|\rho_{21}|v_1)T^*(v_c|\overline{\epsilon}\gamma' l'k_l'|\rho_{21}'|v_1')g(ll'k_lk_l'p_\gamma p_\gamma'k_{10}k_{10}'p_{10}p_{10}'k_{21}k_{21}'p_{21}p_{21}'|\hat{k}),\end{aligned}\tag{34}$$

where

$$G(v_1 v_1' n_i|\Delta t) = \sqrt{\frac{\pi^5}{2}}\varepsilon_{\rm pr}^2 \tau_{\rm pr} f_{\rm pu}(E_1^{v_1} - E_0^{n_i}) f_{\rm pu}(E_1^{v_1'} - E_0^{n_i}) \times \exp\left[-\frac{\tau_{\rm pr}^2}{8}(E_1^{v_1} - E_1^{v_1'})^2\right] \exp[-i(E_1^{v_1} - E_1^{v_1'})\Delta t], \tag{35}$$

$$g(ll' k_l k_l' p_\gamma p_\gamma' k_{10} k_{10}' p_{10} p_{10}' k_{21} k_{21}' p_{21} p_{21}'|\hat{k}) = \frac{1}{8}(-1)^{k_l + k_{10}' + k_{21}'} \frac{\tilde{l}\tilde{l}'}{4\pi} \sum_{J_1, J_2, J} \tilde{J}_1^2 \tilde{J}_2^2 \tilde{J}^2 \begin{pmatrix} 1 & 1 & J_1 \\ 0 & 0 & 0 \end{pmatrix} \begin{pmatrix} 1 & 1 & J_2 \\ 0 & 0 & 0 \end{pmatrix} \begin{pmatrix} j_1 & J_2 & J \\ 0 & 0 & 0 \end{pmatrix} \begin{pmatrix} l & l' & J \\ 0 & 0 & 0 \end{pmatrix} \times {\sum}' \begin{pmatrix} 1 & 1 & J_1 \\ k_{10} & k_{21} & -k_{10} - k_{21} \end{pmatrix} \begin{pmatrix} 1 & 1 & J_2 \\ k_{10}' & k_{21}' & -k_{10}' - k_{21}' \end{pmatrix} \begin{pmatrix} J_1 & J_2 & J \\ k_{10} + k_{21} & -k_{10}' - k_{21}' & k_l' - k_l \end{pmatrix} \times \begin{pmatrix} l & l' & J \\ -k_l & k_l' & k_l - k_l' \end{pmatrix} P_J(\cos\theta_k), \tag{36}$$

and the superscript ST (short time) serves as a reminder that Eq. (34) pertains to delay times shorter than rotational coherence times. The primed summation symbol in Eq. (36) implies summation over all-sign combinations of the k_α ($\alpha = 10, 21, l$), with each term in the summand multiplied by the product of parities $(-1)^{p_\alpha}$ corresponding to the negated k_α (see Appendix B). Equation (36) has a simple interpretation when the 3-j symbols are expressed as vector coupling coefficients [46],

$$\begin{pmatrix} l_1 & l_2 & l_3 \\ m_1 & m_2 & m_3 \end{pmatrix} = (-1)^{l_1 - l_2 - m_3} \frac{1}{\tilde{l}_3} \langle l_1 m_1, l_2 m_2 | l_3 - m_3 \rangle.$$

The 3-j symbols in the third-line couple the excitation and ionization-photon angular momenta while the first 3-j symbol in the last-line couples the two 2-photon routes to give a vector $\vec{J}$ with $J \leq 4$. Conservation of total angular momentum requires that $\vec{J}$ be the vector sum of the electron angular momenta $\vec{l}, \vec{l}'$.

In Eq. (34), the time dependence and the properties of the pump- and probe-pulse envelopes are contained solely in the G while the g describe the dependence of the cross section on the scattering direction. The transition dipole elements, T, couple the time evolution contained in the G with the scattering angle dependence in the g and thus give rise to the change of the asymmetry parameters with time in the course of a nonradiative transition. Equation (34) is a significant result. Namely, it reduces the numerical effort involved in calculation of time-resolved PADs to that required for calculation of time-resolved PEDs.

4. Neglect of vibrations

In order to compute the time-resolved PAD of Eq. (34), one needs to calculate the vibronic field-free Hamiltonian, propagate a large set of coupled differential equations for the nuclear motion (or diagonalize the Hamiltonian) and compute the ionization amplitudes as a function of the internuclear distances. Use of simple-model Hamiltonians (harmonic force fields with linear coupling), similar to those proved successful in energy-domain analysis of nonadiabatic transitions and in the calculation of time-resolved PEDs [16], would eliminate the electronic-structure problem and, by allowing a sparse representation of the field-free Hamiltonian, simplify the dynamical problem. A Franck-Condon approximation (neglect of the **R** dependence of the I) is often justifiable and significantly simplifies the calculation. While feasible for certain types of systems, a time-dependent solution remains a numerical challenge.

Qualitative insight into the type and magnitude of change in the PAD expected to accompany a nonradiative transition can nevertheless be gained by computing the cross section at two time instances; an early time (a pump-probe delay short with respect to the time scale of the nonadiabatic transition), when the electronic character of the wave packet is that of the bright state, and a late time, when the electronic character has been transformed to that of the dark state. For that purpose it suffices to take account of the electronic dynamics, that is, replace the T in Eq. (34) by the electronic bound-free amplitudes, computed at fixed molecular geometries. With vibrations neglected, the cross section reduces to

$$\overline{\overline{\sigma}}_{\xi_1}(\overline{\epsilon}\hat{k}|n_i) = \sum_{\rho_{10}\rho_{10}'} I(\rho_{10}) I^*(\rho_{10}') \times \sum_{\rho_{21}\rho_{21}'} \sum_{\gamma l k_l \gamma' l' k_l'} I_{\xi_1}(\overline{\epsilon}\gamma l k_l|\rho_{21}) I_{\xi_1}^*(\overline{\epsilon}\gamma' l' k_l'|\rho_{21}') g(ll' k_l k_l' p_\gamma p_\gamma' k_{10} k_{10}' p_{10} p_{10}' k_{21} k_{21}' p_{21} p_{21}'|\hat{k}), \tag{37}$$

where the label ξ_1 distinguishes between the two electronic components of the excited manifold, the I are given by Eqs. (22) and (25) and the g are given by Eq. (36).

In Eq. (37) the chemical information is contained in the electronic bound-free amplitudes that embody the symmetries of the bound and free states and the details of the interaction of the electron with the core. The g are analytical functions, correlating the polarization of the excitation and ionization dipole operators and laser fields with the direction of ejection of the photoelectrons. Pictorially, these functions can be thought of as transforming the symmetry of the electronic wave functions with respect to the body-fixed frame into anisotropy of the space-fixed angular distribution. It is worth pointing out that Eq. (37) is not equivalent to a frequency-domain PAD computed with vibrations and rotations neglected since the two-pulse nature of the observable and the relative time scales of the vibronic and rotational motions are implicit in the g.

5. A one-electron approximation

Although Eq. (37) is conceptually transparent, from the numerical view point it still entails the challenge of evaluating the electronic bound-free transition dipole elements. We proceed to approximate the $I_{\xi_1}(\overline{\epsilon\gamma} l k_l|\rho_{21})$ by assuming that ionization takes place via a one-electron process where the core electrons remain unaltered. The single-electron model proved successful in many ionization studies [50,52]. The effects of correlation in ionization of ground states is studied in detail in Ref. [57], where guidelines for the dependence of correlation on the molecular structure are presented. From this study [57] one might conclude that the extent to which correlations play a role is system dependent, although generally minor for outer-shell ionization. A study of correlation effects in ionization of excited states is warranted.

Within a single-electron approximation, Eq. (25) reduces to the matrix element of the dipole operator between the bound and free electronic orbitals involved in the ionization,

$$I_{\xi_1}(\epsilon\gamma l k_l|\rho_{21}) \approx \sqrt{\frac{2}{\pi}}\, i^{-l} \int d\mathbf{Q} \phi^{\gamma *}_{l k_l}(\epsilon\mathbf{Q}) \rho_{21} \phi^{\gamma_{\xi_1}}(\mathbf{Q}), \tag{38}$$

where $\phi^{\gamma_{\xi_1}}$ and $\phi^{\gamma}_{l k_l}$ are bound and free electronic orbitals of IRs γ_{ξ_1} and γ, respectively. The continuum orbital is expanded in generalized harmonics of argument $\hat{Q}$ [49,50] [see Eqs. (15), (26), and Appendix A], ensuring that the $\phi^{\gamma}_{l k_l}(\epsilon\mathbf{Q})$ transform as the γ IR of the point group of the core equilibrium structure. A similar expansion of the bound orbitals proved successful in electron scattering [49] and ionization [50,52] studies of small molecules and has the advantage of allowing analytical calculation of the integral over $\hat{Q}$. Our main interest here, however, is in large, π-conjugated systems of the type discussed in Sec. I. The bound orbitals are thus expressed as a multicenter expansion.

In Eq. (38) the bound state contains the information about the geometry of the molecular configuration and the electronic symmetry of the initial state. The angular part of the free state contains the electronic symmetry of the continuum while its radial part contains the details of the electron-core scattering event and is responsible for the sensitivity of frequency-resolved PADs to the ionization dynamics. It may thus be expected that calculation of absolute asymmetry parameters would be sensitive to the accuracy of the radial electronic wave functions while prediction of the *change* of the β_j accompanying a nonradiative process, the observable of interest in a pump-probe study, would require only proper account of symmetry and angular-momentum algebra. While comparison of approximate with exact calculations or with experimental time-resolved PADs would be essential in order to test this expectation, it is important to keep in mind (see Sec. I) that the usefulness of time-resolved PADs as a probe relies on its validity. In the model calculation discussed in the next section we neglect altogether the ionization dynamics, replacing the radial part of the electron-free wave by its asymptotic form, a scattering Coulomb function of order l [58], $e^{-i\sigma_l}F_l(\eta;kr)$, where $k=\sqrt{2\epsilon}$ is the magnitude of the photoelectron momentum, $\eta=-1/k$ and σ_l is the Coulomb phase shift, $\sigma_l=\arg\Gamma(l+1+i\eta)$. This approximation eliminates system-dependent details and implies that only the change of the PAD upon transition, not its magnitude, can be properly described. Methods of different accuracy for approximating the free-electronic states have been described and could be implemented in the above framework in studies where absolute asymmetry parameters for specific molecules are the goal.

6. Summary

The weak-field approximation of Sec. II B 1 restricts the discussion to pump duration and intensities such that $\tau_{\rm pu} < \Omega_R^{-1}$. Its introduction provides a closed-form expression for the scattering-angle dependence of the observable, Eq. (30).

The slowly varying continuum approximation of Sec. II B 2 is valid provided sharp resonances (of width $\Gamma \lesssim \tau_{\rm pr}^{-1}$) are not accessed by the probe field. Its introduction allows a closed-form expression for the temporal dependence of the PAD, Eq. (32).

The neglect of centrifugal coupling in Sec. II B 3 restricts application to time delays $\Delta t < 2\pi/E^{vJ}$, where E^{vJ} is the rotation-vibration coupling energy [54]. Neglect of the dependence of the eigenvalues on the rotational quantum numbers further restricts the discussion to time delays shorter than rotational periods, $\Delta t < \pi/B_e$. (For the example studied in Sec. III, for instance, the rotational periods are of order 10^{-10} sec while internal conversion takes place on a 10^{-13} sec time scale [20].) The introduction of these approximations allows clear separation of the different processes reflected in the PAD based on their time-scales and provides a basis for interpretation of the results (see Sec. III). From the practical view point, it allows the calculation of the time-resolved PAD at the numerical cost that is involved in the calculation of time-resolved PEDs.

In Sec. II B 4 we sacrificed a detailed solution of the time-dependent entangled vibronic dynamics and focused on predicting the change of the PAD that accompanies a nonradia-

tive transition. For this heavy price the method became applicable to a significantly larger class of molecules.

The range of validity of the one-electron model, Sec. II B 5, depends on both the molecule and the observable and was previously explored [57].

III. EXAMPLE

In this section we apply the formalism of Sec. II to investigate the possibility of using time-resolved PADs to follow the course of a nonadiabatic transition. We use the internal conversion of the transpolyene family, represented here by the eight-carbon member, octatetraene, as an example. Our motivation in the choice of system is three fold. First, we expect an experimental study of the internal conversion of octatetraene by time-resolved PADs to be feasible since the time-resolved PED (for technical reasons, for the methyl-substituted molecule, decatetraene) has already been measured [20]. Second, the bound electronic wave functions of octatetraene are available from semiempirical calculations [20]. Third, the center of inversion of the C_{2h} point-group renders symmetry arguments simple and transparent. It is important to restress that our description of the bound and free electronic wave functions is approximate and, hence, system properties (apart from the underlying symmetries) play a minor role. Our results should thus be considered as appropriate for a general model with the symmetry properties of long-chain transpolyenes.

In the energy domain, the photophysics of transpolyenes has been studied quite intensively [59], this interest arising from the relevance of the nonradiative dynamics of these systems to photobiological processes, such as vision, biological light harvesting, and transmembrane proton pumps, and from their suitability to electronic-structure calculations [60]. The ground $S_0(1A_g)$ state is dipole connected to the second excited $S_2(1B_u)$ state. The latter undergoes internal conversion, promoted by a b_u mode, into a lower-lying singlet state of A_g symmetry, $S_1(2A_g)$. As discussed in Ref. [20], ionization from both bright (S_2) and dark (S_1) states of octatetraene into the ground $[D_0(1B_g)]$ state of the ion is strongly dominated by one-electron processes. The ionized orbital is thus of a_u and b_g symmetries for ionization of the $S_2(1B_u)$ and $S_1(2A_g)$ states, respectively. Using the multiplication table of the C_{2h} point group we find that ionization of the bright state produces free-electron wave functions of b_g symmetry for transitions polarized parallel to the molecular plane and of a_g symmetry for transitions polarized perpendicular to the plane. Ionization of the dark state, by contrast, results in scattering wave functions of a_u and of b_u symmetries for transitions polarized parallel and perpendicular to the molecular plane, respectively.

The photoelectron angular distribution with respect to the molecular frame is readily determined using Eqs. (A5). These distributions are shown in Fig. 1 as a function of the polar (Θ_K) and azimuthal (Φ_K) photoelectron ejection angles. Following the standard conventions we choose the body-fixed Z axis parallel to the C_2 axis, with the central C-C bond defining the Y axis. While the center of inversion of the C_{2h} point group is evident in both P_{1B_u} and P_{2A_g}, the

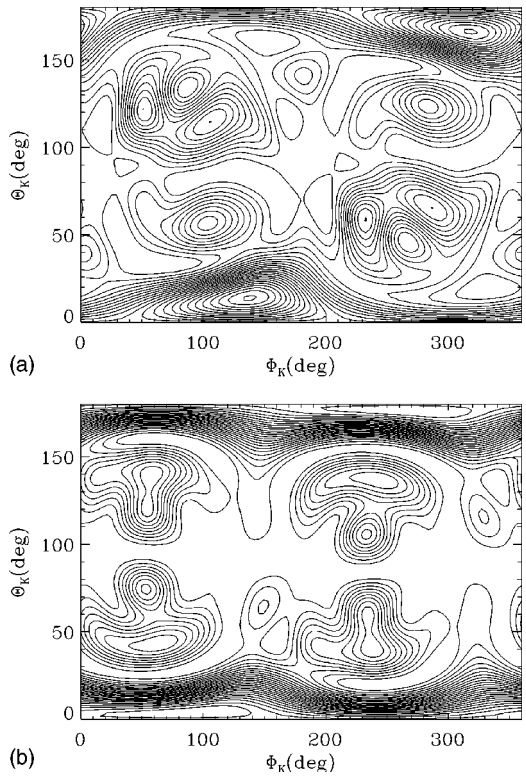

FIG. 1. Body-fixed electron density distributions, P_Γ as functions of the polar (Θ_K) and azimuthal (Φ_K) body-fixed angles for ionization of the bright, $\Gamma=1B_u$ (1a) and dark, $\Gamma=2A_g$ (1b) states of the model transpolyene of Sec. III. P_{1B_u} is peaked off the Z axis with marked asymmetry with respect to $\Theta_K \rightarrow \pi-\Theta_k$ and $\Phi_K \rightarrow 2\pi-\Phi_K$ arising from interference of X, Y, and Z polarized transitions. By contrast, P_{2A_g} is strongly peaked perpendicular to the molecular plane, along the positive and negative Z axes, and nearly symmetric with respect to $\Theta_k \rightarrow \pi-\Theta_K$ and $\Phi_K \rightarrow 2\pi-\Phi_K$, as a consequence of strongly dominating XY-polarized transitions.

distributions differ markedly in detail. The reason is readily understood. Since the octatetraene carbon backbone is planar and rather extended, in-plane (XY) transitions play an important role in both the bright and the dark states ionization processes. For symmetry reasons, however [see Appendix A], in the bright state, only partial waves with $l \geqslant 2$ contribute to plane-polarized transitions, which acts to reduce the dominance of the XY component and give the transition a mixed character. This is observed in Fig. 1(a) where the marked asymmetry with respect to $\Theta_K \rightarrow \pi-\Theta_K$ and $\Phi_K \rightarrow 2\pi-\Phi_K$ arises from interference between XY- and Z-polarized components. By contrast, ionization of the dark state, where odd $l \geqslant 1$ contribute to both XY- and Z-polarized transitions, is strongly dominated by in-plane components. Consequently the body-fixed distribution of Fig. 1(b) is nearly symmetric with respect to both $\Theta_K \rightarrow \pi-\Theta_K$ and $\Phi_K \rightarrow 2\pi-\Phi_K$. A large $\{l>0, k_l=0\}$ component is responsible for the dominant maximum of P_{2A_g} along the Z axis ($\Theta_K=0,\pi$) but the Φ_K structure clearly indicates nonnegligible contribution of up to $k_l=4$ partial waves.

The observable (space-fixed) angular distribution of Eqs.

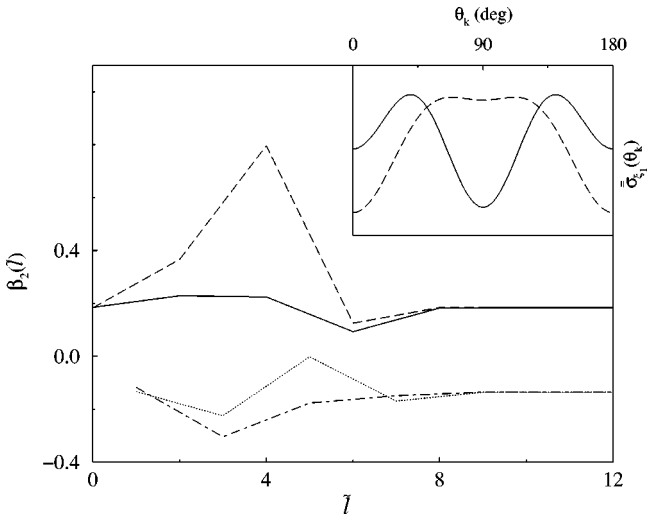

FIG. 2. Space-fixed photoelectron angular distributions [Eqs. (37),(36)] and ionization asymmetry parameters [Eq. (30)], calculated within the short time and neglect of vibrations approximations. The inset shows the PADs for ionization of the $1B_u$ (solid curve) and $2A_g$ (dashed curve) vs the polar photoelectron scattering angle (θ_k). The distributions are normalized so as to allow display on a common scale. The main frame examines the sensitivity of the lower-order asymmetry parameter β_2 [Eq. (30)] to 50% changes in the relative magnitude (solid and dotted curves) and phases (dashed and dotdashed) of the ionization bound-free transition dipole elements, using the procedure discussed in the text. The solid and dashed curves correspond to ionization from the bright state, the dotted and dot-dashed curves to ionization from the dark state. The large $\tilde{l}$ limit of $\beta_2(\tilde{l})$ gives the physical asymmetry parameter for the $1B_u$ (solid and dotted curves) and $2A_g$ (dashed and dotdashed curves). The value of $\tilde{l}$ at which the curve stabilizes indicates the number of partial waves needed to converge the calculation. The deviation from the large $\tilde{l}$ limit shows the effect on β_2 of increasing by 50% the phase or magnitude of one of the partial-wave amplitudes ($l=\tilde{l}$) composing the signal.

(36) and (37) is shown as an inset in Fig. 2 for ionization from the bright (solid curve) and dark (dashed curve) states of octatetraene. The distributions are normalized so as to allow display on a common scale; the overall signal is smaller for the dark state since only one of the three configurations of which the electronic state is composed ionizes into the ground ion state via a one-electron process [20,21]. We stress that only the change of the asymmetry parameters upon internal conversion, not the actual shape of the angular distribution, is of interest for our purpose and can be accounted for by the present method.

The mechanism through which the symmetry difference between the free-electron waves produced through ionization of the $S_2(1B_u)$ and $S_1(2A_g)$ states translates into a marked difference between the corresponding space-fixed angular distributions is readily visualized. For the specific case of transpolyenes the excitation is polarized in the molecular plane and hence the pump pulse prepares an anisotropic distribution of magnetic states, broadly aligned (as $\sin^2\theta$) perpendicular to the common polarization axis of the pump and probe fields. Since the molecules do not rotate appreciably during the short delay times considered, the dominating maximum of the charge distribution along the body-fixed Z axis in Fig. 1(b) is directly observed in the laboratory frame as a peak of the dark-state PAD perpendicular to the polarization vector, $\theta_k=\pi/2$ (dashed curve in the inset of Fig. 2). Similarly, the minimum of the charge distribution of Fig. 1(a) along the Z axis translates into a minimum of the corresponding space-fixed distribution at $\theta_k=\pi/2$ (solid curve in the inset of Fig. 2). We expect that for other systems different (noncollinear) relative orientation of the pump and probe polarization vectors would serve better to unravel the difference in electronic symmetry between the coupled Born-Oppenheimer states.

Since our numerical method of computing the radial components of the electronic bound-free amplitudes is approximate, it is germaine to investigate the sensitivity of the outcome to the relative magnitude and relative phase of the partial-wave amplitudes composing the signal. The main body of Fig. 2 shows the asymmetry parameter β_2 [see Eq. (30)] computed with systematically modified radial amplitudes. The solid and dotted curves give $\beta_2(\tilde{l})$ computed with the modulus of the $l=\tilde{l}$ partial-wave amplitude, $|I_{\xi_1}(\epsilon\gamma\tilde{l}k_l|\rho_{21})|$, increased by 50%. The moduli of all $l\neq\tilde{l}$ partial-wave amplitudes and the phases of all amplitudes are unaltered. The dashed and dot-dashed curves give $\beta_2(\tilde{l})$ calculated with $\arg\{I_{\xi_1}(\epsilon\gamma\tilde{l}k_l|\rho_{21})\}$ increased by 50%, the arguments of all $I_{\xi_1}(\epsilon\gamma l\neq\tilde{l}k_l|\rho_{21})$ being kept at their correct value. The solid and dashed curves correspond to ionization from the bright state while the dotted and dot-dashed ones correspond to ionization from the dark state.

Figure 2 serves several purposes. The large $\tilde{l}$ limit of $\beta_2(\tilde{l})$ gives the physical asymmetry parameter within the present model. The deviation from this value for a given $\tilde{l}$ measures the relative contribution of the $\tilde{l}$ partial wave to the PAD and the value of $\tilde{l}$ at which the curve stabilizes indicates the number of partial waves needed to converge the calculation. Figure 2 suggests that errors in the relative magnitude and, more so, in the relative phase of the bound-free amplitudes may produce significant errors in the computed asymmetry parameters. They do not, however, modify the qualitative information sought.

Our present results pertain to the golden-rule limit, where the alignment induced by the pump field is limited by the single-photon selection rules to be very mild, proportional to $\cos^2\theta$ ($\sin^2\theta$) for excitation transitions polarized parallel (perpendicular) to the symmetry (C_2) axis. In short-pulse experiments, the golden-rule limit pertains to the case where the pulse is shorter than the Rabi period, $\tau<\Omega_R^{-1}$, where Ω_R, the Rabi coupling, is proportional to the field strength. As shown in Ref. [56], much sharper alignment than that attained in the weak-field limit can be achieved by choosing $\tau>\Omega_R^{-1}$, whereby Rabi cycling between the initial and excited states produces broad-rotational wave packets in both states. In practice rotational excitation is usually easier to induce than to avoid. The above discussion suggests the exciting opportunity of using a moderately intense pump field

to enhance the change of the PAD that occurs in the course of a symmetry changing transition. A similar enhancement can be achieved by using a third, nonresonant [61] laser to align the system. The latter scheme would have an advantage in cases where an intense pump field involves the risk of two-photon ionization of the ground state. We expect that in some cases, depending on the molecular symmetry and the nature of the bound-bound transition, the natural (pump-induced) alignment would not be helpful and prealignment of the molecule with a nonresonant pulse of appropriate polarization would be necessary in order to translate the symmetry change into a laboratory frame observable.

IV. CONCLUSION

Our goal in this study has been to investigate formally and numerically the capability of time-resolved PADs to provide a useful view of nonradiative transitions in large polyatomic systems. To that end we first extended the formalism developed in Ref. [39] for calculation of time-resolved PADs in linear systems to apply to general polyatomic molecules and reformulated the observables so as to expose the underlying electronic and rotational symmetries. By invoking a sequence of approximations we next reduced the formally exact expressions successively to cruder forms that are applicable to systems of increasing complexity. Our final-result entails gross approximation of the ionization dynamics but is capable of extracting the essential physics while remaining numerically trivial. In particular, it illustrates the mechanism through which a change in the electronic symmetry in the course of an internal conversion or an intersystem crossing translates into a drastic change of the observable PAD.

We focused on the development of physically transparent expressions that could be applied to gain qualitative insight into the type of information contained in femtosecond-resolved PADs, and into the time scale on which different phenomena are expected to appear. Application was limited to a single system and only briefly discussed. Specifically, we considered the internal conversion dynamics of a trans-linear-polyene predicting a significant change of the asymmetry parameters for ionization into the ground ion state upon conversion of the $S_2(1B_u)$ into the $S_1(2A_g)$ state.

It is clear that much remains to be accomplished. Application of the formalism derived here to a variety of systems of different symmetries and transition-types would be essential in order to examine the generality of the method, its range of applicability and its limitations. This work is currently underway.

A second task of future work would be to refine the model by eliminating one or more of the approximations involved, as appropriate for the application considered.

(1) The development or adaptation of improved methods for computing electronic scattering wave functions that remain applicable to systems of the size discussed in Sec. I, would permit quantitative calculation of the PAD at fixed delay times, Sec. II B 4.

(2) More interesting would be the application of Eq. (34) to compute the PAD as a function of the time delay, taking into explicit account the vibronic dynamics. As noted in Sec. II B 3, by restricting attention to time delays shorter than rotational coherence times, Eq. (34) reduces the numerical effort involved in the calculation of time-resolved PADs to that required for calculation of time-resolved PEDs. The latter observable has been already computed for large molecules undergoing internal conversion [16]. While simplification of the vibronic Hamiltonian and neglect of all but the dominating modes would be typically inevitable, such approximations are often justifiable through time-scale arguments.

(3) Although the main focus of the present work has been the problem of electronic coupling, the formalism of Sec. II and Appendixes B–D is general and could be applied to predict the effect of other perturbations on time-resolved PADs from polyatomic molecules. A case of interest is the onset of rotation-vibration coupling, studied experimentally in Ref. [27] and examined theoretically for diatomic systems in Refs. [11,28]. This task requires relaxing the approximation of Sec. II B 3 and implementing the formalism of Sec. II B 1. It entails, however, the simplification that calculation of the electronic bound-free amplitudes is usually unnecessary.

(4) An exciting opportunity that remains to be explored is that of using a moderately intense pump field to improve the alignment induced during the excitation pulse, thus enhancing the change of the PAD in the course of the transition. A similar effect can be achieved with a third, far-off-resonance intense field. To examine this possibility it would be necessary to go beyond the golden-rule approximation of Sec. II B 1 and treat the field nonperturbatively, as detailed in Sec. II A.

The experimental technology for measuring the effects predicted here is currently available. We hope that the present results would assist in the design of future experiments and in the choice of systems and expect such experiments to pose new questions for theoretical research.

Further information about wave packet dynamics, beyond that available through resolution of the photoelectrons with respect to energy and angle, is contained in the observables of time-resolved photoelectron-photoion coincidence imaging spectroscopy [37,62]. The technology required for such measurements was recently developed and tested [37,62]. An interesting problem for theoretical research is thus the investigation of the type and quality of new (not available from more conventional observables) information that could be gained from energy- and angle-resolved photoelectron-photoion coincidence measurements in the time domain. This may be expected to go beyond the realization of a molecule-fixed PAD [62]. The extension of the present formalism to that end forms another avenue for future research.

ACKNOWLEDGMENTS

It is a pleasure to thank Marek Zgierski, Albert Stolow, James Shaffer, Jonathan Underwood, and Michael Schmitt for many interesting conversations. I am grateful to Marek Zgierski for providing me with the bound electronic states of octatetraene and to Albert Stolow, Jonathan Underwood, and Phil Bunker for reading the manuscript and for making helpful comments.

APPENDIX A: FORM OF THE GENERALIZED HARMONICS FOR POINT GROUPS LACKING AXES OF SYMMETRY OF ORDER HIGHER THAN 2

In this Appendix, we derive explicit expressions for the generalized harmonics of Eq. (15) for the title point groups (point groups C_2, C_i, C_{2h}, D_2, C_{2v} and D_{2h}) [51]. We focus on these groups since the systems discussed in the introduction all belong to one of them and since the lack of axis of symmetry of order higher than 2 in these groups simplifies the form of the $X_{kl}^{\gamma\mu}$, giving expressions whose symmetry properties are readily visualized.

The symmetry operations to be considered are thus [44,55] two-fold rotations about three mutually orthogonal axes, C_{2X}, C_{2Y}, C_{2Z}, reflections, σ_{XY}, σ_{XZ}, σ_{YZ}; and inversion, i. Under these operations the spherical harmonics transform as

$$\begin{aligned} C_{2X}Y_{lk_l}&=(-1)^l Y_{l-k_l},\\ C_{2Y}Y_{lk_l}&=(-1)^{l-k_l}Y_{l-k_l},\\ C_{2Z}Y_{lk_l}&=(-1)^{k_l}Y_{lk_l},\\ \sigma_{XY}Y_{jk_l}&=(-1)^{l+k_l}Y_{lk_l},\\ \sigma_{XZ}Y_{lk_l}&=(-1)^{k_l}Y_{l-k_l}, \end{aligned} \tag{A1}$$

$$\sigma_{YZ}Y_{lk_l}=Y_{l-k_l},$$

and

$$iY_{lk_l}=(-1)^l Y_{lk_l}. \tag{A2}$$

Consequently, all IRs of the title point groups transform under the respective group's symmetry operations as

$$X_{lk_l}^{\gamma}=\frac{1}{\sqrt{2}}(Y_{lk_l}+(-1)^{p_\gamma}Y_{l-k_l}). \tag{A3}$$

With Eqs. (A1)–(A3), generalized harmonics for the IRs of the above point groups are readily constructed. For the specific case of the C_{2h} point group, considered in Sec. III, the group symmetry operations do not mix Y_{lk_l} with Y_{l-k_l} and hence the spherical harmonics provide an appropriate basis. It is nevertheless convenient to expand the electronic state in real and imaginary linear combinations of the form (A4). Using the C_{2h} character table and Eqs. (A1)–(A3) we have,

$$\begin{aligned} X_{lk_l}^{a_g}&=\sqrt{2}Y_{lk_l}(\Theta_K,0)\cos(k_l\Phi_K); \quad i\sqrt{2}Y_{lk_l}(\Theta_K,0)\sin(k_l\Phi_K),\ l\ \text{even},\ k_l\ \text{even},\\ X_{lk_l}^{b_g}&=i\sqrt{2}Y_{lk_l}(\Theta_K,0)\sin(k_l\Phi_K); \quad \sqrt{2}Y_{lk_l}(\Theta_K,0)\cos(k_l\Phi_K),\ l\ \text{even},\ k_l\ \text{odd},\\ X_{lk_l}^{a_u}&=\sqrt{2}Y_{lk_l}(\Theta_K,0)\cos(k_l\Phi_K); \quad i\sqrt{2}Y_{lk_l}(\Theta_K,0)\sin(k_l\Phi_K),\ l\ \text{odd},\ k_l\ \text{even},\\ X_{lk_l}^{b_u}&=i\sqrt{2}Y_{lk_l}(\Theta_K,0)\sin(k_l\Phi_K); \quad \sqrt{2}Y_{lk_l}(\Theta_K,0)\cos(k_l\Phi_K),\ l\ \text{odd},\ k_l\ \text{odd}. \end{aligned} \tag{A4}$$

APPENDIX B: INTEGRATION OVER THE EULER ANGLES IN EQS. (18) AND (19)

In this Appendix, we provide explicit expressions for the integrals over the Euler angles of rotation, W in Eqs. (18) and (19), and their reduced forms w appearing in Eqs. (29), (31), and (33). These expressions are used in the derivation of sum rules in Appendices C and D below. In order to simplify the notation we confine attention to the point-groups discussed in Appendix A, where Eq. (15) takes the form (27), and neglect spin. At the end of the Appendix, we outline the extension of the expressions to the general case of Eqs. (20) and (23).

Consider first the excitation (bound-bound) integral in Eq. (18). Using Eqs. (11)–(13) and Eq. (3.118) of Ref. [46] we have

$$\begin{aligned} &W(J_1\tau_1M_1p_1|k_{10}qp_{10}|J_0\tau_0M_0p_0)\\ &\quad=\sqrt{\frac{8\pi^2}{3}}\int d\hat{R}\langle\hat{R}|J_1\tau_1M_1p_1\rangle^*\\ &\qquad\times\langle\hat{R}|1k_{10}qp_{10}\rangle\langle\hat{R}|J_0\tau_0M_0p_0\rangle\\ &\quad=(-1)^{M_1}\begin{pmatrix} J_1 & 1 & J_0\\ M_1 & -q & -M_0\end{pmatrix}\\ &\qquad\times w(J_1\tau_1p_1|k_{10}p_{10}|J_0\tau_0p_0), \end{aligned} \tag{B1}$$

where

$$w(J_1\tau_1 p_1|k_{10}p_{10}|J_0\tau_0 p_0)=\frac{\tilde{J}_1\tilde{J}_0}{\sqrt{8}}\sum_{K_1K_0} a_{J_1\tau_1K_1}a_{J_0\tau_0K_0}(-1)^{K_1}$$
$$\times\left\{\begin{pmatrix} J_1 & 1 & J_0 \\ K_1 & -k_{10} & -K_0\end{pmatrix}+(-1)^{p_1}\begin{pmatrix} J_1 & 1 & J_0 \\ -K_1 & -k_{10} & -K_0\end{pmatrix}+(-1)^{p_{10}}\begin{pmatrix} J_1 & 1 & J_0 \\ K_1 & k_{10} & -K_0\end{pmatrix}\right.$$
$$\left.+(-1)^{p_0}\begin{pmatrix} J_1 & 1 & J_0 \\ K_1 & -k_{10} & K_0\end{pmatrix}\right\}[1+(-1)^{J_0+p_0+1+p_{10}+J_1+p_1}]. \tag{B2}$$

The angular integral appearing in the bound-free matrix element, Eq. (19), is written as

$$W(J_c\tau_c M_c p_c|lk_l m_l p_\gamma|k_{21}qp_{21}|J_1\tau_1 M_1 p_1)$$
$$=\sqrt{\frac{8\pi^2}{3}\frac{8\pi^2}{2l+1}}\int d\hat{R}\langle\hat{R}|J_c\tau_c M_c p_c\rangle^*\langle\hat{R}|lk_l m_l p_\gamma\rangle^*\langle\hat{R}|1k_{21}qp_{21}\rangle\langle\hat{R}|J_1\tau_1 M_1 p_1\rangle$$
$$=\sum_{J_2,M_2}\begin{pmatrix} J_c & l & J_2 \\ M_c & m_l & M_2\end{pmatrix}\begin{pmatrix} J_2 & 1 & J_1 \\ M_2 & q & M_1\end{pmatrix}w(J_2|J_c\tau_c p_c|lk_l p_\gamma|k_{21}p_{21}|J_1\tau_1 p_1), \tag{B3}$$

where

$$w(J_2|J_c\tau_c p_c|lk_l p_\gamma|k_{21}p_{21}|J_1\tau_1 p_1)$$
$$=\frac{\tilde{J}_c\tilde{J}_1\tilde{J}_2^2}{4}\sum_{K_cK_1} a_{J_c\tau_cK_c}a_{J_1\tau_1K_1}\{\omega(K_c,k_l,k_{21},K_1)+(-1)^{p_c}\omega(-K_c,k_l,k_{21},K_1)$$
$$+(-1)^{p_\gamma}\omega(K_c,-k_l,k_{21},K_1)+(-1)^{p_{21}}\omega(K_c,k_l,-k_{21},K_1)+(-1)^{p_1}\omega(K_c,k_l,k_{21},-K_1)$$
$$+(-1)^{p_c+p_\gamma}\omega(-K_c,-k_l,k_{21},K_1)+(-1)^{p_c+p_{21}}\omega(-K_c,k_l,-k_{21},K_1)$$
$$+(-1)^{p_c+p_1}\omega(-K_c,k_l,k_{21},-K_1)\}[1+(-1)^{J_c+p_c+l+p_\gamma+1+p_{21}+J_1+p_1}], \tag{B4}$$

and

$$\omega(K_c,k_l,k_{21},K_1)=\sum_{K_2}\begin{pmatrix} J_c & l & J_2 \\ K_c & k_l & K_2\end{pmatrix}\begin{pmatrix} J_2 & 1 & J_1 \\ K_2 & k_{21} & K_1\end{pmatrix}. \tag{B5}$$

The factors $[1+(-1)^{J_0+p_0+1+p_{10}+J_1+p_1}]$ in Eq. (B2) and $[1+(-1)^{J_c+p_c+l+p_\gamma+1+p_{21}+J_1+p_1}]$ in Eq. (B4) ensure that the integrals of Eqs. (B1) and (B3) vanish unless the corresponding integrands are invariant under the symmetry operations of the D_2 group.

Very similar expressions are obtained in the general case of Eqs. (20) and (23) where, however, the J and their space-fixed projections are replaced by the respective angular momenta excluding spin and their projections and, since the $\sqrt{8\pi^2/2l+1}<\hat{R}|lm_l k_l p_\gamma\rangle^*$ in Eq. (B3) is replaced by $D^l_{m_l k_l}$, the W are independent of γ.

APPENDIX C: DERIVATION OF EQ. (29)

Substituting Eqs. (18), (19), (B1), and (B3) in Eq. (28), collecting terms dependent on M_i and M_c and, for notational simplicity, assuming both pump and probe fields to be linearly polarized along a common axis, we denote

$$\mathcal{S}\equiv\sum_{M_iM_c}\begin{pmatrix} J_c & l & J_2 \\ M_c & m_l & -M_i\end{pmatrix}\begin{pmatrix} J_2 & 1 & J_1 \\ -M_i & 0 & M_i\end{pmatrix}$$
$$\times\begin{pmatrix} J_1 & 1 & J_i \\ M_i & 0 & -M_i\end{pmatrix}\begin{pmatrix} J_c & l' & J_2' \\ M_c & m_l' & -M_i\end{pmatrix}$$
$$\times\begin{pmatrix} J_2' & 1 & J_1' \\ -M_i & 0 & M_i\end{pmatrix}\begin{pmatrix} J_1' & 1 & J_i \\ M_i & 0 & -M_i\end{pmatrix}. \tag{C1}$$

Using Eqs. (2.30), (2.31), and (4.16) of Ref. [46] we expand two pairs of the 3-j symbols in Eq. (C1) as

$$\begin{pmatrix} J_2 & 1 & J_1 \\ -M_i & 0 & M_i\end{pmatrix}\begin{pmatrix} J_1 & 1 & J_i \\ M_i & 0 & -M_i\end{pmatrix}$$
$$=(-1)^{J_2+1+M_i}\sum_{j_1}\tilde{J}_1{}^2\begin{Bmatrix} 1 & J_2 & J_1 \\ J_i & 1 & j_1\end{Bmatrix}$$
$$\times\begin{pmatrix} 1 & 1 & j_1 \\ 0 & 0 & 0\end{pmatrix}\begin{pmatrix} J_2 & J_i & j_1 \\ M_i & -M_i & 0\end{pmatrix} \tag{C2}$$

and

$$\begin{pmatrix} J_2' & 1 & J_1' \\ -M_i & 0 & M_i \end{pmatrix}\begin{pmatrix} J_1' & 1 & J_i \\ M_i & 0 & -M_i \end{pmatrix} = (-1)^{J_2'+1+M_i}\sum_{j_2}\tilde{J}_2^2\begin{Bmatrix} 1 & J_2' & J_1' \\ J_i & 1 & j_2 \end{Bmatrix} \times\begin{pmatrix} 1 & 1 & j_2 \\ 0 & 0 & 0 \end{pmatrix}\begin{pmatrix} J_2' & J_i & j_2 \\ M_i & -M_i & 0 \end{pmatrix}. \quad \text{(C3)}$$

Equation (4.16) of Ref. [46] is next used to couple Eqs. (C2) and (C3),

$$\begin{pmatrix} J_2 & J_i & j_1 \\ M_i & -M_i & 0 \end{pmatrix}\begin{pmatrix} J_2' & J_i & j_2 \\ M_i & -M_i & 0 \end{pmatrix} = (-1)^{J_2+J_i+J_2'+M_i}\sum_{j}\tilde{J}^2\begin{Bmatrix} j_1 & J_2 & J_i \\ J_2 & j_2 & j \end{Bmatrix} \times\begin{pmatrix} j_1 & j_2 & j \\ 0 & 0 & 0 \end{pmatrix}\begin{pmatrix} J_2 & J_2' & j \\ M_i & -M_i & 0 \end{pmatrix} \quad \text{(C4)}$$

and the sum over M_i and M_c is carried out by application of Eq. (4.15) [46],

$$\sum_{M_iM_c}(-1)^{M_i}\begin{pmatrix} J_c & l & J_2 \\ M_c & m_l & -M_i \end{pmatrix} \times\begin{pmatrix} J_c & l' & J_2' \\ M_c & m_l' & -M_i \end{pmatrix}\begin{pmatrix} J_2 & J_2' & j \\ M_i & -M_i & 0 \end{pmatrix} = (-1)^{J_c+m_l}\begin{Bmatrix} l & J_2 & J_c \\ J_2' & l' & j \end{Bmatrix}\begin{pmatrix} l' & l & j \\ -m_l' & m_l & 0 \end{pmatrix}\delta_{m_l,m_l'}. \quad \text{(C5)}$$

Hence,

$$\mathcal{S} = (-1)^{J_i+J_c+m_l}\sum_{j_1j_2=0,2}\sum_{j=0,2,4}\tilde{J}_1^2\tilde{J}_2^2\tilde{J}^2 \times\begin{pmatrix} 1 & 1 & j_1 \\ 0 & 0 & 0 \end{pmatrix}\begin{pmatrix} 1 & 1 & j_2 \\ 0 & 0 & 0 \end{pmatrix}\begin{pmatrix} j_1 & j_2 & j \\ 0 & 0 & 0 \end{pmatrix} \times\begin{Bmatrix} 1 & 1 & j_1 \\ J_2 & J_i & J_1 \end{Bmatrix}\begin{Bmatrix} 1 & 1 & j_2 \\ J_2' & J_i & J_1' \end{Bmatrix}\begin{Bmatrix} j_1 & j_2 & j \\ J_2' & J_2 & J_i \end{Bmatrix} \times\begin{Bmatrix} l & l' & j \\ J_2' & J_2 & J_c \end{Bmatrix}\begin{pmatrix} l & l' & j \\ m_l & -m_l & 0 \end{pmatrix}, \quad \text{(C6)}$$

where we noted the symmetry properties of the six-j symbols, Eqs. (4.9) of Ref. [46]. Using Eqs. (2.32), (3.94), and (3.116) of Ref. [46], the m_l-dependent terms in the cross section are cast in the form,

$$\sum_{m_l}(-1)^{m_l}Y_{lm_l}(\hat{k})Y_{l'm_l}^*(\hat{k})\begin{pmatrix} l & l' & j \\ m_l & -m_l & 0 \end{pmatrix} = \frac{\tilde{l}\tilde{l}'}{4\pi}\begin{pmatrix} l & l' & j \\ 0 & 0 & 0 \end{pmatrix}P_j(\cos\theta_k) \quad \text{(C7)}$$

with $j=0,2,4$.

Substituting Eqs. (18), (19), (B1), and (B3) in Eq. (28) and using Eqs. (C1), (C6), and (C7) we obtain Eq. (29) in the text with F_j defined as,

$$F_j(J_iJ_1J_1'll'J_2J_2'J_c) = \frac{(-1)^{J_i+J_c}}{2J_i+1}\frac{\tilde{l}\tilde{l}'}{4\pi}\sum_{j_1j_2=0,2}\tilde{J}_1^2\tilde{J}_2^2\tilde{J}^2\begin{pmatrix} 1 & 1 & j_1 \\ 0 & 0 & 0 \end{pmatrix} \times\begin{pmatrix} 1 & 1 & j_2 \\ 0 & 0 & 0 \end{pmatrix}\begin{pmatrix} j_1 & j_2 & j \\ 0 & 0 & 0 \end{pmatrix}\begin{Bmatrix} 1 & 1 & j_1 \\ J_2 & J_i & J_1 \end{Bmatrix} \times\begin{Bmatrix} 1 & 1 & j_2 \\ J_2' & J_i & J_1' \end{Bmatrix}\begin{Bmatrix} j_1 & j_2 & j \\ J_2' & J_2 & J_i \end{Bmatrix}\begin{Bmatrix} l & l' & j \\ J_2' & J_2 & J_c \end{Bmatrix} \times\begin{pmatrix} l & l' & j \\ 0 & 0 & 0 \end{pmatrix}. \quad \text{(C8)}$$

APPENDIX D: DERIVATION OF EQ. (34)

In this Appendix we derive angular momentum sum rules that allow the summation over the ion rotational indices in Eq. (8) as well as the coherent sums over the intermediate rotational levels in Eqs. (31) to be carried out analytically, provided that the dynamical process studied is fast with respect to rotational periods and that symmetric top systems are considered. As discussed in Sec. II B 3, in this limit the dependence on rotational quantum numbers is contained only in analytical functions; the w of Eqs. (B2) and (B4) and the F_j defined by Eq. (C8).

Collecting the J_c-dependent terms in Eqs. (B4) and (C8) we have,

$$\sum_{J_c}(-1)^{J_c}\tilde{J}_c^2\begin{Bmatrix} l & l' & j \\ J_2' & J_2 & J_c \end{Bmatrix}\begin{pmatrix} J_c & l & J_2 \\ K_c & k_l & K_2 \end{pmatrix}\begin{pmatrix} J_c & l' & J_2' \\ K_c & k_l' & K_2' \end{pmatrix} = (-1)^{l+l'+J_2+J_2'+K_2'+k_l}\begin{pmatrix} l & l' & j \\ -k_l & k_l' & k_l-k_l' \end{pmatrix} \times\begin{pmatrix} J_2' & J_2 & j \\ K_2' & -K_2 & k_l'-k_l \end{pmatrix}, \quad \text{(D1)}$$

where we used Eq. (4.16) of Ref. [46]. The J_1-dependent terms in Eqs. (B2), (B4), and (C8) are next be summed as,

$$\sum_{J_1} \tilde{J}_1^2 \begin{Bmatrix} 1 & 1 & j_1 \\ J_2 & J_i & J_1 \end{Bmatrix} \begin{pmatrix} J_1 & 1 & J_i \\ K_1 & -k_{10} & -K_i \end{pmatrix} \begin{pmatrix} J_2 & 1 & J_1 \\ K_2 & k_{21} & K_1 \end{pmatrix}$$
$$= (-1)^{J_2+k_{10}+K_2+1} \begin{pmatrix} 1 & 1 & j_1 \\ -k_{10} & -k_{21} & k_{10}+k_{21} \end{pmatrix} \times \begin{pmatrix} J_2 & J_i & j_1 \\ -K_2 & -K_i & -k_{10}-k_{21} \end{pmatrix}, \quad \text{(D2)}$$

and similarly

$$\sum_{J_1'} \tilde{J}'^2_1 \begin{Bmatrix} 1 & 1 & j_2 \\ J_2' & J_i & J_1' \end{Bmatrix} \begin{pmatrix} J_1' & 1 & J_i \\ K_1' & -k_{10}' & -K_i \end{pmatrix} \begin{pmatrix} J_2' & 1 & J_1' \\ K_2' & k_{21}' & K_1' \end{pmatrix}$$
$$= (-1)^{J_2'+k_{10}'+K_2'+1} \begin{pmatrix} 1 & 1 & j_2 \\ -k_{10}' & -k_{21}' & k_{10}'+k_{21}' \end{pmatrix} \times \begin{pmatrix} J_2' & J_i & j_2 \\ -K_2' & -K_i & -k_{10}'-k_{21}' \end{pmatrix}. \quad \text{(D3)}$$

The selection rule $k_{10}+k_{21}-k_{10}'-k_{21}'=k_l=k_l'$ follows from the properties of the terminal 3-j symbols in Eqs. (D1)–(D3). With Eqs. (D1)–(D3) we are in position to perform the sum over J_2 in Eq. (31),

$$\sum_{J_2} \tilde{J}_2^2 \begin{Bmatrix} j_1 & j_2 & j \\ J_2' & J_2 & J_i \end{Bmatrix} \begin{pmatrix} J_2' & J_2 & j \\ K_2' & -K_2 & k_l'-k_l \end{pmatrix} \times \begin{pmatrix} J_2 & J_i & j_1 \\ -K_2 & -K_i & -k_{10}-k_{21} \end{pmatrix}$$
$$= (-1)^{J_2'+K_2'+K_i+K_2} \begin{pmatrix} J_2' & J_i & j_2 \\ K_2' & K_i & k_{10}'+k_{21}' \end{pmatrix} \times \begin{pmatrix} j_1 & j_2 & j \\ k_{10}+k_{21} & -k_{10}'-k_{21}' & k_l'-k_l \end{pmatrix}. \quad \text{(D4)}$$

Finally

$$\sum_{J_2'} (-1)^{J_2'} \tilde{J}_2'^2 \begin{pmatrix} J_2' & J_i & j_2 \\ -K_2' & -K_i & -k_{10}'-k_{21}' \end{pmatrix} \times \begin{pmatrix} J_2' & J_i & j_2 \\ K_2' & K_i & k_{10}'+k_{21}' \end{pmatrix} = (-1)^{J_i} \quad \text{(D5)}$$

where we used the orthogonality property of the 3-j symbols, Eq. (2.33) of Ref. [46]. Substituting Eqs. (B2), (B4), (C8), and (D1)–(D5) in Eq. (31) one obtains Eq. (34).

[1] A. H. Zewail, *Femtochemistry: Ultrafast Dynamics of the Chemical Bond* (World Scientific, Singapore, 1994); D. Zhong and A. H. Zewail, J. Phys. Chem. A **102**, 4031 (1998).

[2] *Femtosecond Chemistry*, edited by J. Manz and L. Wöste (Weinheim, Basel, 1995).

[3] P. Y. Cheng, D. Zhong, and A. H. Zewail, J. Chem. Phys. **105**, 6216 (1996).

[4] D. M. Neumark, Annu. Rev. Phys. Chem. **52**, 255 (2001) and references therein.

[5] C. C. Hayden and A. Stolow, in *Photoionization and Photodetachment*, edited by C.-Y. Ng, Advanced Series in Physical Chemistry Vol. 10A (World Scientific, Singapore, 1999), and references therein.

[6] T. Baumert, J. Helbing, and G. Gerber, Adv. Chem. Phys. **101**, 47 (1997) and references therein.

[7] W. Domcke and G. Stock, in *Advances in Physical Chemistry Vol. 100* (Wiley, New York, 1997), and references therein.

[8] R. M. Williams, J. M. Papanikolas, J. Rathje, and S. R. Leone, J. Chem. Phys. **106**, 8310 (1997).

[9] J. H. D. Eland, *Photoelectron Spectroscopy* (Butterworths, London, 1984).

[10] Ultrafast spin dynamics and spin-dependent electron dynamics have been observed in femtosecond studies in metals, A. Scholl, L. Baumarten, R. Jacquemin, and W. Eberhardt, Phys. Rev. Lett. **79**, 5146 (1997); M. Aeschlimann *et al.*, *ibid.* **79**, 5158 (1997).

[11] T. Seideman and S. C. Althorpe, J. Electron Spectrosc. Relat. Phenom. **108**, 99 (2000).

[12] A. Assion, M. Geiseler, J. Helbiing, V. Seyfried, and T. Baumert, Phys. Rev. A **54**, R4605 (1996).

[13] Ch. Meier and V. Engel, in *Femtosecond Chemistry* (Ref. [2]), p. 369.

[14] K. Resch, V. Blanchet, A. Stolow, and T. Seideman, J. Phys. Chem. A **105**, 2756 (2001).

[15] B. Kim, C. P. Schick, and P. M. Weber, J. Chem. Phys. **103**, 6903 (1995).

[16] (a) G. Stock, R. Schneider, and W. Domcke, J. Chem. Phys. **90**, 7184 (1989); (b) M. Seel and W. Domcke, *ibid.* **95**, 7806 (1991); (c) S. Krempl, W. Domcke, and M. Winterstetter, Chem. Phys. **206**, 63 (1996).

[17] C. C. Hayden and D. W. Chandler, J. Phys. Chem. **99**, 7897 (1995); D. R. Cyr and C. C. Hayden, J. Chem. Phys. **10**, 771 (1996).

[18] W. Radloff, V. Stert, Th. Freudenberg, I. V. Hertel, C. Jouvet, C. Dedonder-Lardeux, and D. Solgadi, Chem. Phys. Lett. **281**, 20 (1997).

[19] C. P. Schick, S. D. Carpenter, and P. M. Weber, J. Phys. Chem. A **103**, 10 470 (1999).

[20] V. Blanchet, M. Zgierski, T. Seideman, and A. Stolow, Nature (London) **402**, 52 (1999).

[21] V. Blanchet, S. Lochbrunner, M. Schmitt, J. P. Schaffer, J. J. Larsen, M. Zgierski, T. Seideman, and A. Stolow, Faraday Discuss. **115**, 33 (2000).

[22] For a review of the theory of time-resolved PADs, see T. Seideman, Annu. Rev. Phys. Chem. (to be published).

[23] S. W. Allendorf, D. J. Leahy, D. C. Jacobs, and R. N. Zare, J. Chem. Phys. **91**, 2216 (1989); D. J. Leahy, K. L. Reid, H. Park, and R. N. Zare, *ibid.* **97**, 4948 (1992); H. Park and R. N. Zare, *ibid.* **106**, 2239 (1997).

[24] K. L. Reid, Chem. Phys. Lett. **215**, 25 (1993).
[25] K. L. Reid, S. P. Duxon, and M. Towrie, Chem. Phys. Lett. **228**, 351 (1994).
[26] T. Noguchi, S. Sato, and Y. Fujimura, Chem. Phys. Lett. **155**, 177 (1989).
[27] K. L. Reid, T. A. Field, M. Towrie, and P. Matousek, J. Chem. Phys. **111**, 1438 (1999).
[28] S. C. Althorpe and T. Seideman, J. Chem. Phys. **113**, 7901 (2000).
[29] T. Seideman, J. Chem. Phys. **113**, 1677 (2000).
[30] C. C. Hayden (unpublished).
[31] A. Stolow (private communications); A. Sanov (private communications).
[32] Several of the historical reviews about nonradiative transitions are given in: (a) J. Jortner, S. A. Rice, and R. M. Hochstrasser, Adv. Photochem. **7**, 149 (1969); (b) B. R. Henry and W. Siebrand, in *Molecular Luminescence*, edited by E. C. Lim (Benjamin, New York, 1969) p. 423; (c) E. C. Lim, in *Molecular Luminescence* [Ref. 32(b)], p. 469; (d)M. A. El-Sayed, in Molecular Luminescence [Ref. 32(b)], p. 715; (e) K. F. Freed, in *Radiationless Processes in Molecules and Condensed Phases*, edited by F. K. Fong (Springer, Berlin, 1976), p. 23.
[33] As stated in [Ref. 32(a)], ''all photochemical reactions depend, in some step of the mechanism, on the existence of one or more radiationless processes.''
[34] R. W. Schoenlein, L. A. Peteanu, R. A. Mathies, and C. V. Shank, Science **254**, 412 (1991).
[35] J. Jortner and M. Ratner, *Molecular Electronics* (Blackwell, Oxford, 1997).
[36] Femtosecond-resolved photoelectron imaging experiments were reported by L. Wang, H. Kohguchi, and T. Suzuki, Faraday Discuss. **113**, 37 (1999).
[37] Femtosecond photoelectron-photoion coincidence experiments were reported by J. A. Davies, J. E. LeClaire, R. E. Continetti, and C. C. Hayden, J. Chem. Phys. **111**, 1 (1999). See also Ref. [62].
[38] A related ongoing experiment is described by M. J. J. Vrakking, Faraday Discuss. **115**, 90 (2000).
[39] T. Seideman, J. Chem. Phys. **107**, 7859 (1997).
[40] S. C. Althorpe and T. Seideman, J. Chem. Phys. **110**, 147 (1999).
[41] Y. Arasaki, K. Takatsuka, K. Wang, and V. McKoy, Chem. Phys. Lett. **302**, 363 (1999).
[42] By ''rigid'' one refers to molecules for which tunneling between equivalent equilibrium conformations does not take place on the time scale of the experiment, see Ref. [44] p. 5,6. It is important to note that this definition of a rigid molecule allows nonzero vibration amplitude and centrifugal distortion. We note also that molecules may well behave as rigid on the time-scale of a short pulse pump-probe experiment even if analysis of a CW spectrum requires that large amplitude motion be taken into account.
[43] We distinguish between the subscript 0, which labels the energy levels and magnetic states of the initial electronic state, and the subscript *i*, which labels the energy level and magnetic state of the initial rovibrational level, since a nonperturbative field excites in general a wave packet of n_0 and M_0 levels.
[44] G. Herzberg, *Molecular Spectra and Molecular Structure III: Electronic Spectra and Electronic Structure of Polyatomic Molecules* (Van Nostrand Reinhold, New York, 1966).
[45] R. S. Mulliken, Phys. Rev. **59**, 873 (1941).
[46] R. N. Zare, *Angular Momentum. Understanding Spatial Aspects in Chemistry and Physics* (Wiley, New York, 1988).
[47] A. R. Edmonds, *Angular Momentum in Quantum Mechanics*, 2nd ed. (Princeton University Press, Princeton, 1960).
[48] F. C. Von Der Lage and H. A. Bethe, Phys. Rev. **71**, 612 (1947).
[49] P. G. Burke, N. Chandra, and F. A. Gianturco, J. Phys. B **5**, 2212 (1972).
[50] N. Chandra, J. Phys. B **20**, 3405 (1987).
[51] It is more precise to consider the molecular point group as the group of vibronic symmetry operations of a rigid molecule, whereas the symmetry group of the full molecular Hamiltonian is referred to as the ''molecular symmetry group'' in Ref. [55]. Thus, the operations of the molecular point group do not transform the Euler angles. In the case of rigid [42] nonlinear molecules considered here the molecular symmetry group is isomorphic to the molecular point group and hence we prefer the standard usage of ''point group'' for the ''molecular symmetry group.''
[52] N. Chandra, J. Phys. B **20**, 3417 (1987); N. Chandra, J. Chem. Phys. **89**, 5987 (1988); N. Chandra and M. Chakrabory, *ibid.* **95**, 6382 (1991).
[53] For a derivation see, e.g., T. Seideman, Chem. Phys. Lett. **253**, 279 (1996).
[54] M. R. Aliev and J. K. G. Watson, J. Mol. Spec. **3**, 1 (1988).
[55] P. R. Bunker and P. Jensen, *Molecular Symmetry and Spectroscopy* (NRC Research Press, Ottawa, 1998).
[56] T. Seideman, J. Chem. Phys. **103**, 7887 (1995).
[57] L. S. Cederbaum, W. Domcke, J. Schirmer, and W. Von Niessen, Adv. Chem. Phys. **65**, 115 (1986).
[58] M. Abramowitz, in *Handbook of Mathematical Functions*, edited by M. Abramowitz and I. A. Stegun, Applied Math Series 55 (National Bureau of Standards, Washington D.C., 1972).
[59] See, for instance, H. Petek *et al.*, J. Chem. Phys. **102**, 4726 (1994).
[60] For a review see, G. Orlandi, F. Zerbetto, and M. Z. Zgierski, Chem. Rev. **91**, 867 (1991).
[61] B. Friedrich and D. Herschbach, Phys. Rev. Lett. **74**, 4623 (1995); H. Sakai, C. P. Safvan, J. J. Larsen, K. M. Hilligse, K. Hald, and H. Stapelfeldt, J. Chem. Phys. **110**, 10 235 (1999); J. J. Larsen, K. Hald, N. Bjerre, H. Stapelfeldt, and T. Seideman, Phys. Rev. Lett. **85**, 2470 (2000).
[62] J. A. Davis, R. E. Continetti, D. W. Chandler, and C. C. Hayden, Phys. Rev. Lett. **84**, 5983 (2000).